

LUMINOSITY MEASUREMENT AND CALIBRATION AT THE LHC

W. Kozanecki, IRFU-SPP

CEA-Saclay, 20 February 2017

Outline

2

- Introduction: the basics
- Relative-luminosity monitoring strategies
- Absolute-luminosity calibration strategies – & their challenges
- Instrumental systematics in the high- \mathcal{L} environment
- Achieved precision on \mathcal{L} - and why it matters
- Summary
- Selected bibliography

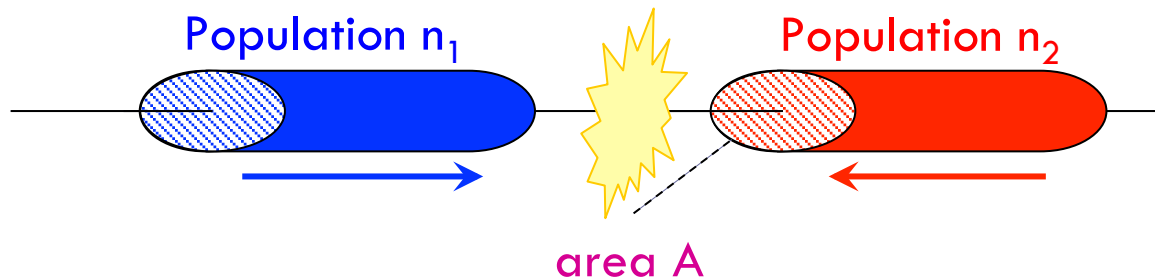
Luminosity: definition

3

The key parameter for the experiments is the event rate R [events/s].
For a physics process with cross-section σ , R is proportional to the luminosity \mathcal{L} :

$$R = \sigma \mathcal{L}$$

unit of \mathcal{L} :
 $1/(\text{surface} \times \text{time})$



$$\text{Collision rate} \propto \sigma \times \underbrace{\frac{n_1 \times n_2}{A} \times \text{encounters/second}}_{\mathcal{L} \text{ (goal: } \pm 1-2 \% \text{)}}$$

Basics of \mathcal{L} measurement: Rate = $\sigma * \mathcal{L}$

4

$$\boxed{\mathcal{L}} = \frac{\boxed{R}}{\sigma} = \frac{\boxed{\mu n_b f_r}}{\sigma_{inel}} = \frac{\boxed{\epsilon \mu} n_b f_r}{\boxed{\epsilon} \sigma_{inel}} = \frac{\boxed{\mu_{eff}} n_b f_r}{\boxed{\sigma_{eff}}}$$

μ = number of inelastic pp collisions per bunch crossing

n_b = number of colliding bunch pairs

f_r = LHC revolution frequency (11245 Hz)

σ_{inel} = total inelastic pp cross-section (~ 80 mb at 13 TeV)

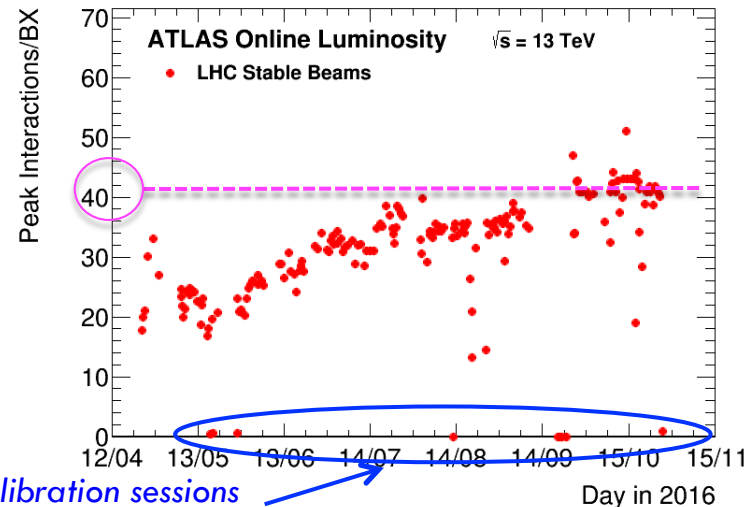
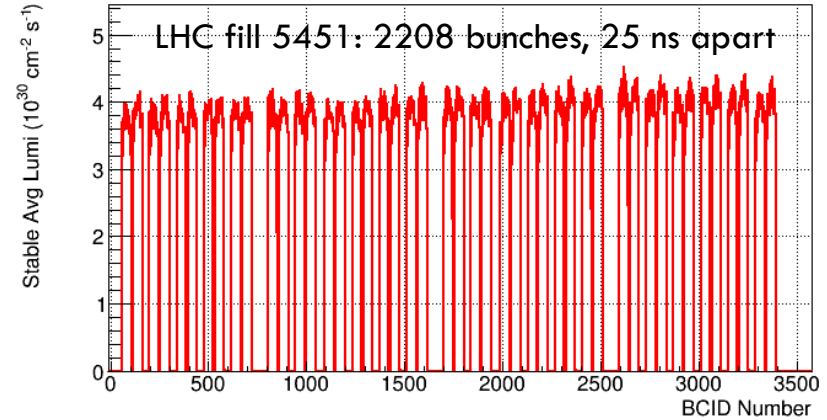
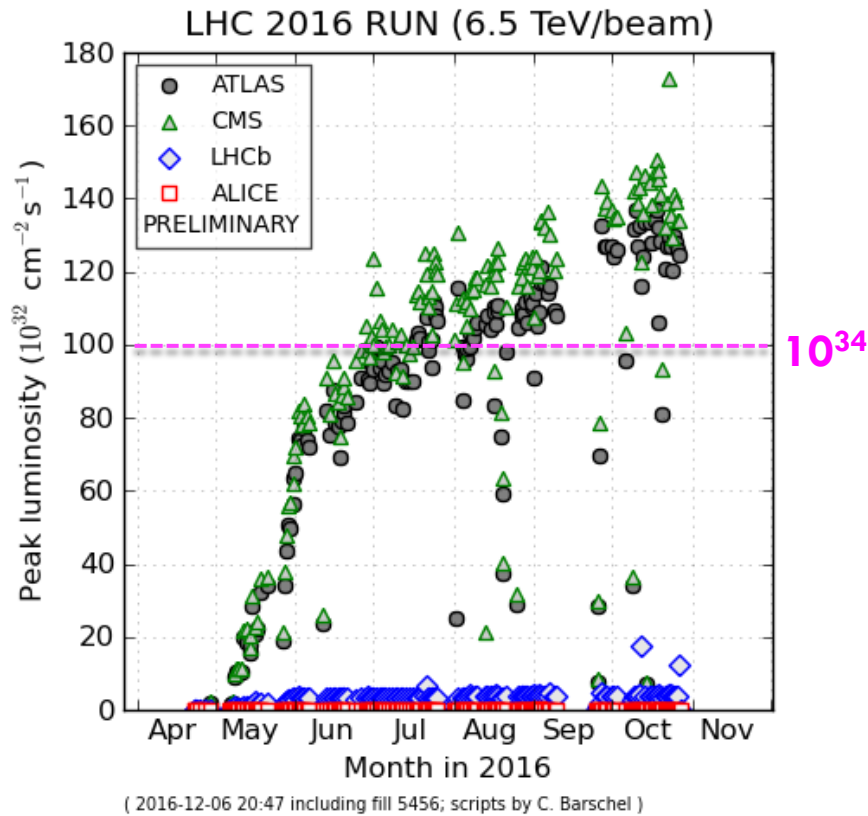
ϵ = acceptance x efficiency of luminosity detector

μ_{eff} = # visible (= detected) collisions per bunch crossing

σ_{eff} = effective cross-section = luminosity calibration constant

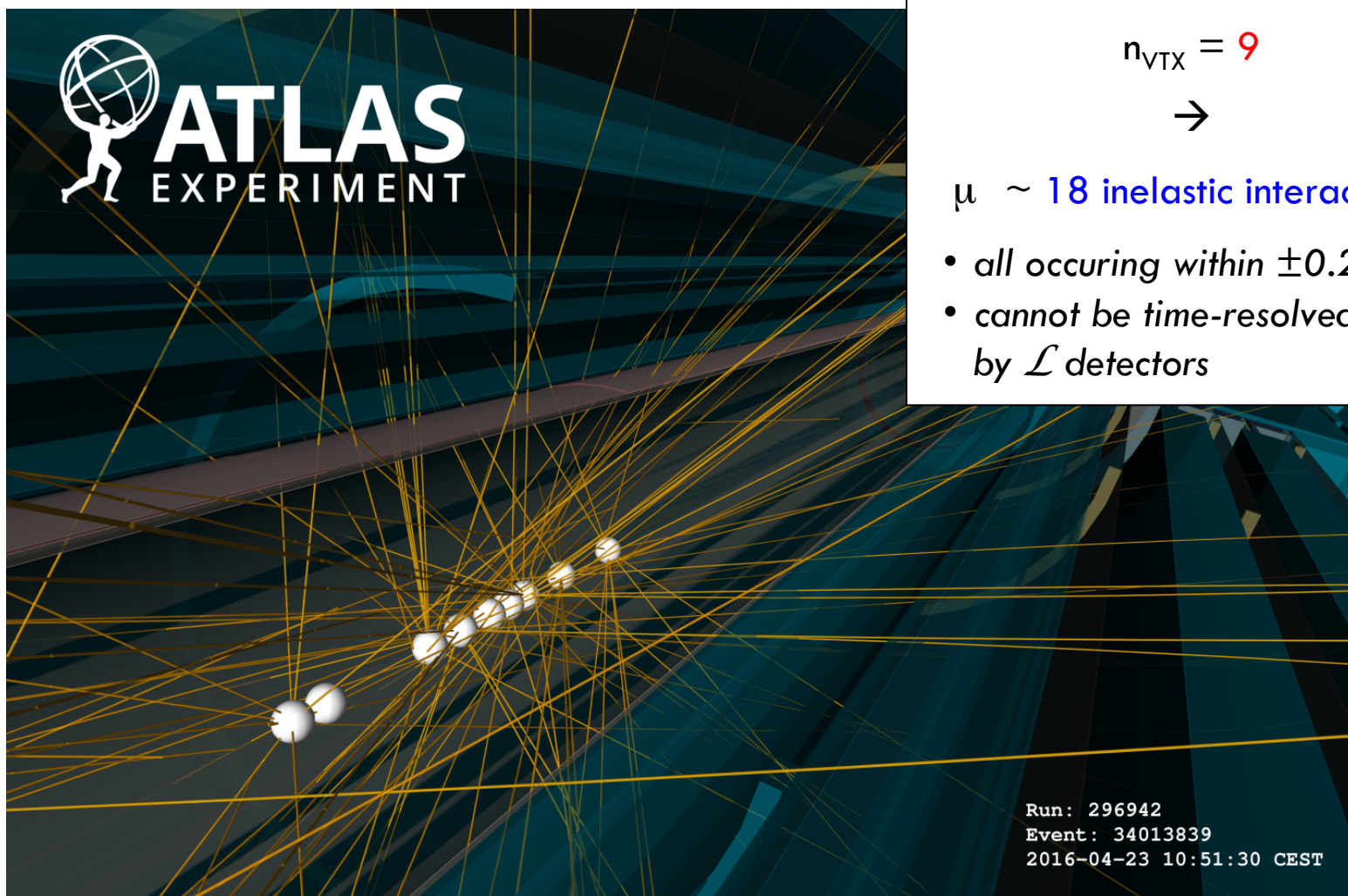
The experimental environment

5



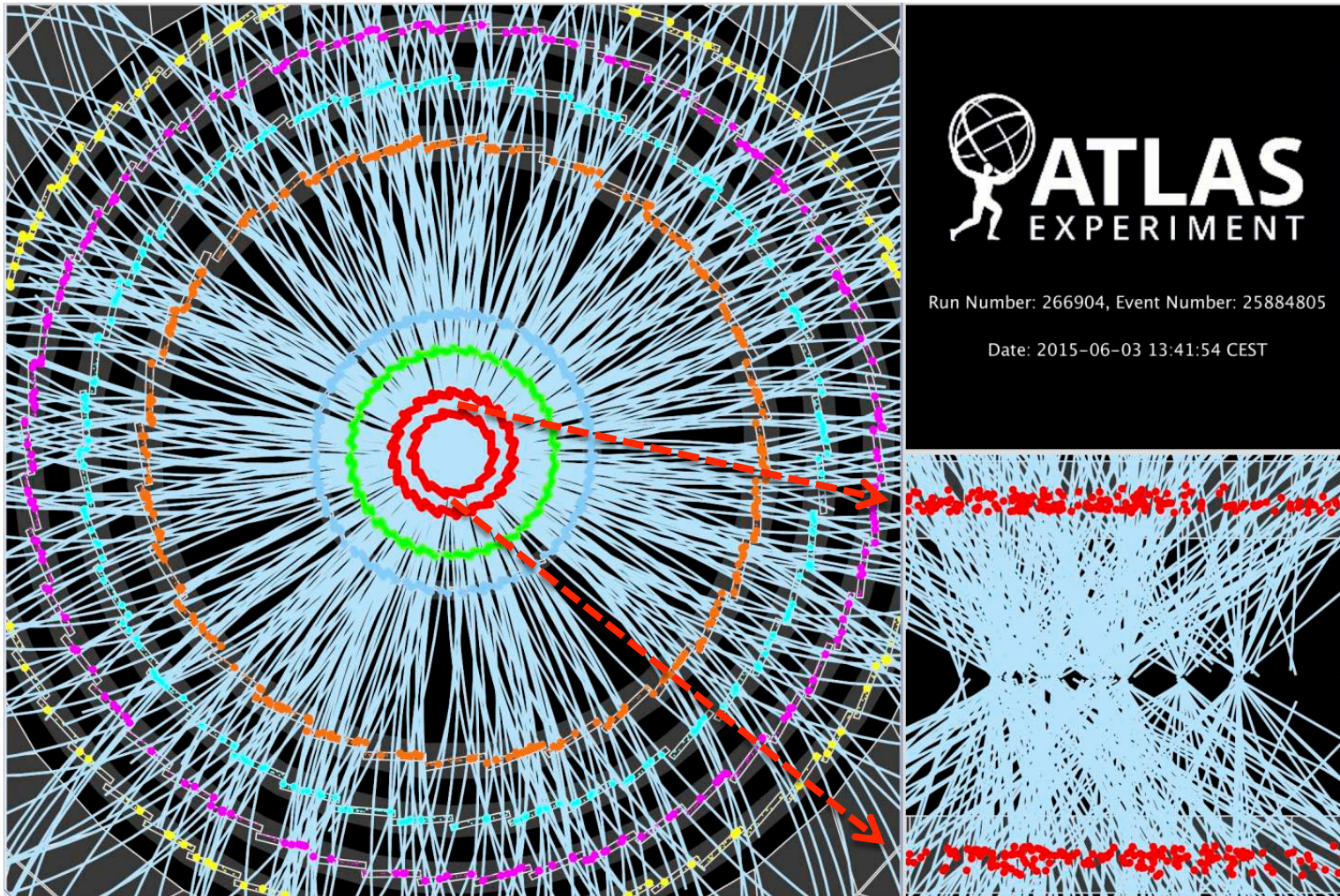
A key issue: the pile-up [Sp̄pS; Tevatron; LHC]

6



Pile-up: a more typical event

7



$n_{\text{VTX}} = 17$
 $\mu \sim 34$

Handling the pile-up: principle

8

- **Event- (or zero-) counting:** bunch-by-bunch (bbb)
 - an “event” is a bunch crossing (BX) where a given condition is satisfied, e.g.:
 - EventOR = at least 1 hit in either the A arm of a luminometer, or the C arm, or both
 - EventAND (aka A.C) = at least 1 hit in the A-arm AND at least 1 hit in the C arm
 - count the fraction of BX with zero events $\rightarrow \mu$ from Poisson probability
 - If μ is the average number of inelastic pp collisions/BX, and N_{OR} (N_{AND}) the total number of OR (AND) “events” over N_{orbits} , then (for 1 colliding bunch pair) the Poisson probability P to detect an “event”/BX is

$$\left\{ \begin{array}{l} P_{OR} = \frac{N_{OR}}{N_{orbits}} = 1 - e^{-\mu \epsilon_{OR}} \\ P_{AND} = \frac{N_{AND}}{N_{orbits}} = 1 - e^{-\mu \epsilon_A} - e^{-\mu \epsilon_C} + e^{-\mu \epsilon_{OR}} \end{array} \right.$$

$$\begin{aligned} \mathcal{L} &\sim \mu = -\ln(1 - P_{OR}) / \epsilon_{OR} \\ &\sim P_{OR} / \epsilon_{OR} \text{ only when } \mu \ll 1 \end{aligned}$$

- examples: $V0_{A.C}$ (ALICE), LUCID_Bi_ORA (ATLAS), ≥ 2 VELO tracks (LHCb)

\mathcal{L} -monitoring algorithms: rate ~~\neq~~ $\sigma_{\text{eff}} * \mathcal{L} ?$ *Pile-up!*

9

- **Event- (or zero-) counting** algorithms: bunch-by-bunch (bbb)
 - count the fraction of BX with zero “events” $\rightarrow \mu$ from Poisson probability
 - \mathcal{L} is a monotonic (but non-linear) function of the “event” rate
 - if μ gets too large, no empty events \rightarrow “zero starvation” or “saturation”
- **Hit-counting** algorithms (bbb) *Now: ATLAS: # LUCID hits. CMS: # pixel clusters.*
 - count the fraction of channels hit in a given BX
 - Poisson formalism, very similar to that of event counting
 - linearity vs. μ depends on technology, granularity, thresholds, ...
- **Track- (& vertex-) counting** algorithms: bbb, *but TDAQ-limited*
 - conceptually similar to hit-counting. Examples: ATLAS, LHCb
- **Flux-counting** algorithms (summed over all bunches)
 - example: current in ATLAS hadronic-calorimeter photomultipliers (PMTs)

ATLAS: redundancy \rightarrow many \mathcal{L} msmts!

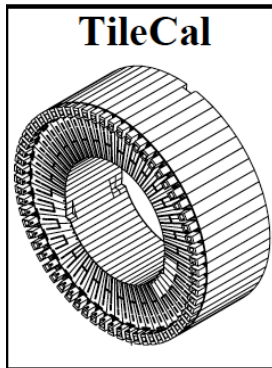
10

Note: all luminometers are independent of TDAQ (exc. trk-, vtx- & Z-counting)

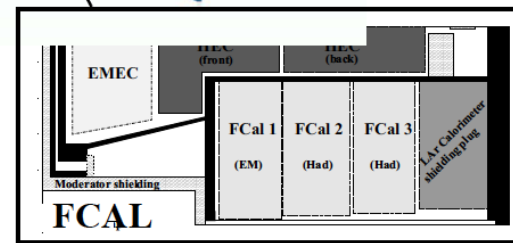
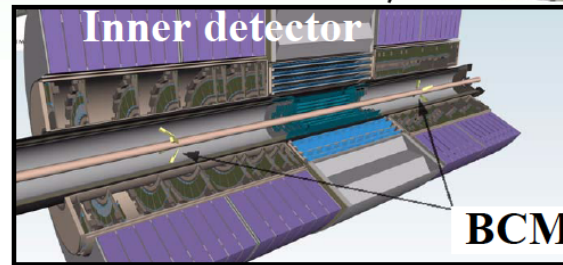
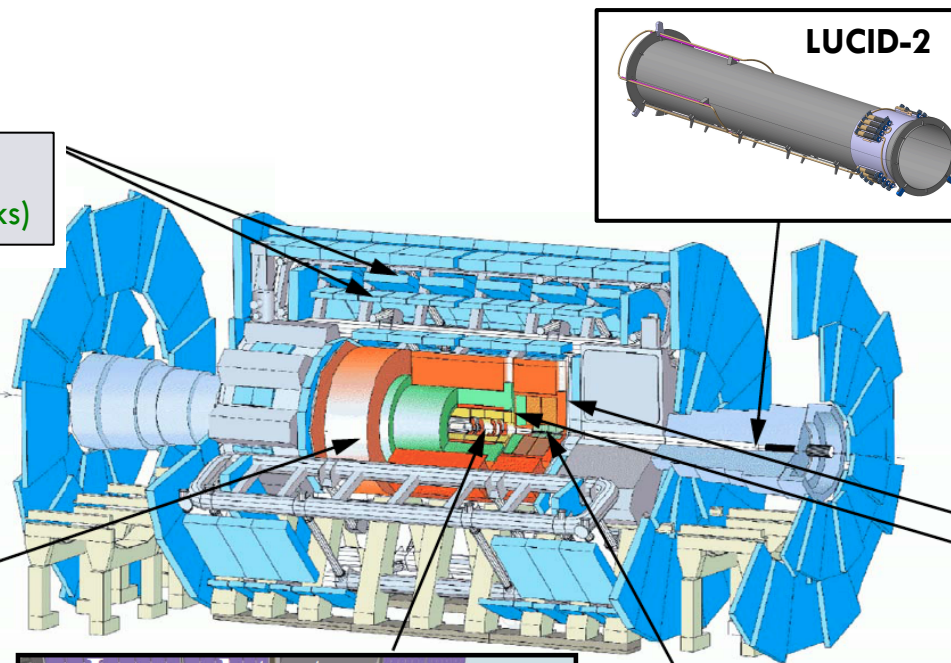
LUCID – Luminosity measurement using a Cherenkov Integrating Detector (bbb)

\rightarrow “ATLAS-preferred” for 13 TeV pp data

+ Z counting (relative- \mathcal{L} checks)



+ Vertex counting
+ Track counting (both bbb)



BCM – Beam Conditions Monitor (bbb)

\rightarrow “ATLAS-preferred” for 7 & 8 TeV pp data

\mathcal{L} -monitoring: instrumental strategies

11

	Preferred offline ($\rightarrow \mathcal{L}_{\text{phys}}$) luminometer	Main addtn'l luminometers: offline corrections + systs.
ALICE	V0 (scintillator arrays): A.C T0 (Cherenkov arrays): A.C + ΔT cut ZDC (had. cal): EventOR (Pb-Pb only)	AD ("diffractive" scint. arrays): A.C μ- & drift-corrected using:
ATLAS	LUCID-2 (quartz Cherenkov +PMTs): HitOR [hit counting, 2-arm inclusive]	Si tracker: track counting EM/Fwd calorimeter: current in LAr gaps TILE hadronic calorimeter: PMT currents
CMS / TOTEM	Si tracker: pixel-cluster counting (PCC)	Pixel \mathcal{L} telescope: evt cntg [3-fold AND] Muon Drift Tubes : track-segment cntg Fwd calorimeter (HF): hit counting
LHCb	VELO tracker: track-based event counting	VELO tracker: vertex-based evt counting PU & SPD arrays: hit counting Calorimeters (+ SPD): energy $> E_{\text{thresh}}$

Absolute- \mathcal{L} calibration: the *initial* plan

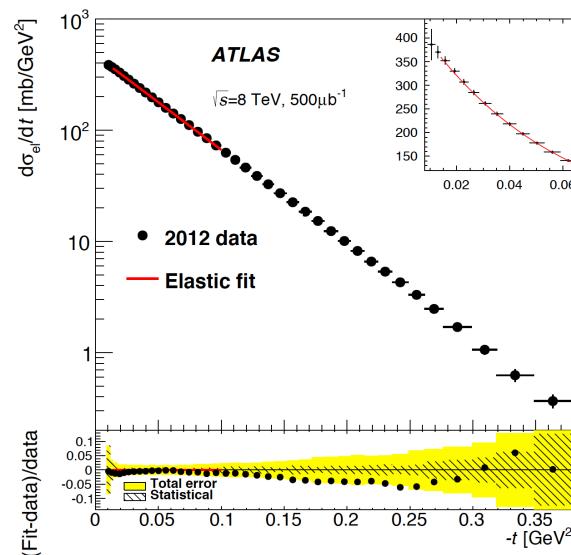
12

- Optical theorem + $pp \rightarrow pp$ (elastic) at low t

$$\sigma_{tot} = 4\pi \text{Im} [f_{el}(t=0)]$$

- ▣ $dR_{el}/dt + R_{inel}$ ($R_{tot} = R_{el} + R_{inel}$) [TOTEM + ALFA]

$$\sigma_{tot} = \frac{16\pi}{1 + \rho^2} \frac{(dR_{el}/dt)_{t=0}}{R_{tot}} \quad \mathcal{L} = \frac{1 + \rho^2}{16\pi} \frac{R_{tot}^2}{(dR_{el}/dt)_{t=0}}$$



Absolute- \mathcal{L} calibration: the *initial* plan

13

- Optical theorem + $pp \rightarrow pp$ (elastic) at low t

$$\sigma_{tot} = 4\pi \text{Im} [f_{el}(t=0)]$$

- ▣ $dR_{el}/dt + R_{inel}$ ($R_{tot} = R_{el} + R_{inel}$) [TOTEM + ALFA]

$$\sigma_{tot} = \frac{16\pi}{1 + \rho^2} \frac{(dR_{el}/dt)_{t=0}}{R_{tot}} \quad \mathcal{L} = \frac{1 + \rho^2}{16\pi} \frac{R_{tot}^2}{(dR_{el}/dt)_{t=0}}$$

- ▣ dR_{el}/dt in Coulomb-interference region [ALFA + TOTEM]

$$\frac{dR_{el}}{dt} = \pi \mathcal{L} |f_C + f_{el}|^2 = \pi \mathcal{L} \left| -\frac{2\alpha}{|t|} + \frac{\sigma_{tot}}{4\pi} (i + \rho) e^{-b|t|/2} \right|^2$$

- $d\sigma_{el}/dt, \sigma_{el}$ msrd at $\sqrt{s} = 7+8$ [+13] TeV (ALFA, TOTEM)

- ▣ but \mathcal{L} -indep. method \rightarrow only loose x-check (3.8 % so far)

Absolute- \mathcal{L} calibration: actual strategy

14

Principle: $\sigma_{\text{eff}} = R_{\text{collisions}} / \mathcal{L}$ (beam parameters)

- van der Meer scans: $\mathcal{L} = f(\Sigma_x, \Sigma_y, n_1, n_2)$ $\Sigma_x \sim (\sigma_{1x}^2 + \sigma_{2x}^2)^{1/2}$
 - ▣ $\Sigma_{x,y}$ from R vs. **beam sep.** $(\delta x, \delta y)$; $n_1, n_2 =$ bunch currents
 - + exploit luminous-region evolution in scan: (δ_x, δ_y) dependence of 3-d position, angles & width of luminous region (aka “beamspot”)
- Beam-gas imaging: $\mathcal{L} = f(\sigma_{x1}, \sigma_{y1}, \sigma_{x2}, \sigma_{y2}, \sigma_z, \phi_c, n_1, n_2)$
 - ▣ extract single-beam parameters from (x, y, z) distribution of reconstructed p-gas & pp evt vertices (stationary beams)
- Beam-beam imaging: $\mathcal{L} = f(\sigma_{x1}, \sigma_{y1}, \sigma_{x2}, \sigma_{y2}, \dots, n_1, n_2)$
 - ▣ scan B1 as a probe across B2 & v-v \rightarrow single-beam parms
 - closely related to luminous-region evolution method in vdM scans

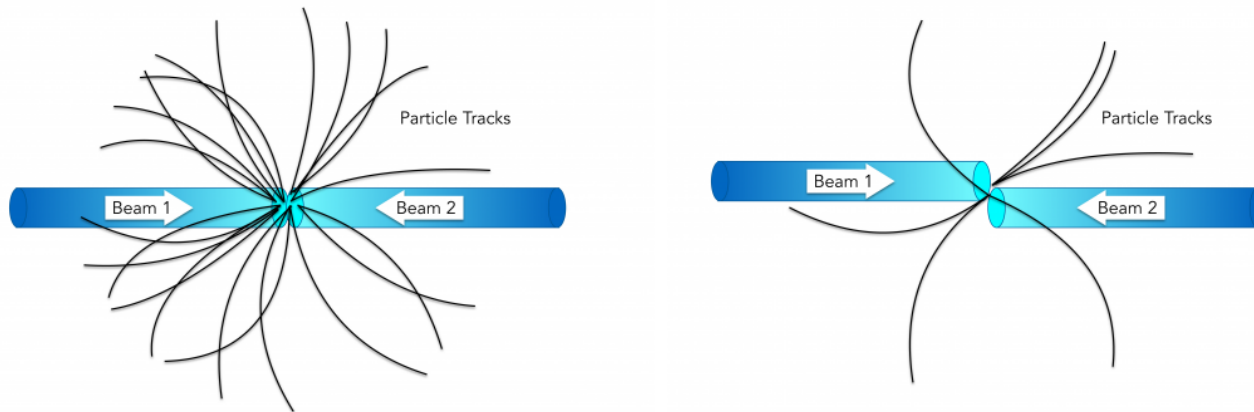
\mathcal{L} calibration: van der Meer scans

15

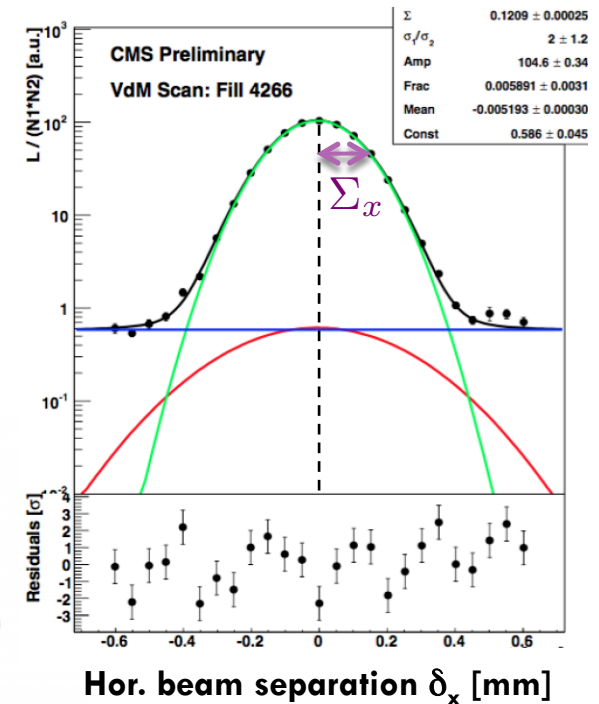
- Measure **visible interaction rate** μ_{eff} as a function of beam separation δ
- The measured reference luminosity is given by

$$\mathcal{L} = \frac{n_b f_r n_1 n_2}{2\pi \Sigma_x \Sigma_y}$$

with $\Sigma_{x,y}$ = integral under the scan curve / peak
 = RMS of scan curve (if Gaussian)



When the two beams overlap completely there are many interactions and many tracks. When the proton beams only overlap slightly there are few interactions and few tracks.



\mathcal{L} calibration: van der Meer scans

16

- Measure **visible interaction rate** μ_{eff} as a function of beam separation δ
- The measured reference luminosity is given by

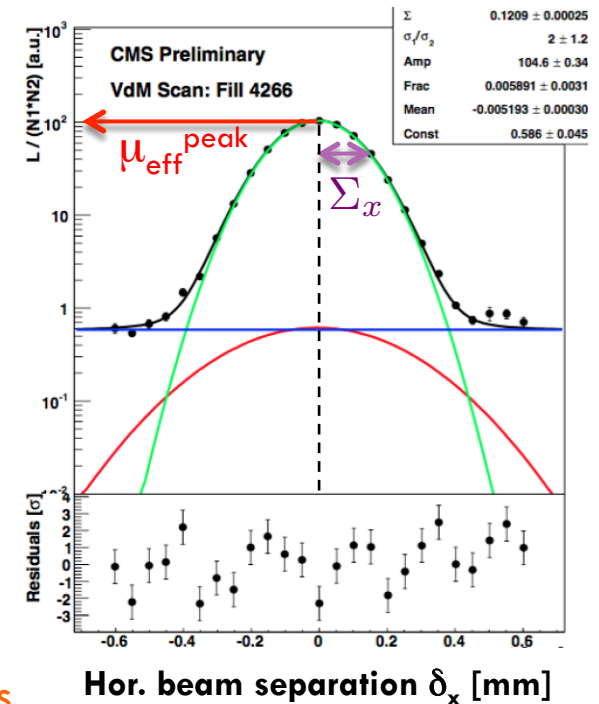
$$\mathcal{L} = \frac{n_b f_r n_1 n_2}{2\pi \Sigma_x \Sigma_y}$$

with $\Sigma_{x,y}$ = integral under the scan curve / peak

- This allows a direct calibration of the **effective cross section** σ_{vis} for each luminosity detector/algorithm

effective cross-section

$$\sigma_{\text{eff}} = \underbrace{\mu_{\text{eff}}^{\text{peak}}}_{\text{peak rate}} \frac{2\pi \underbrace{\Sigma_x \Sigma_y}_{\text{scan widths}}}{\underbrace{n_1 n_2}_{\text{bunch populations}}}$$



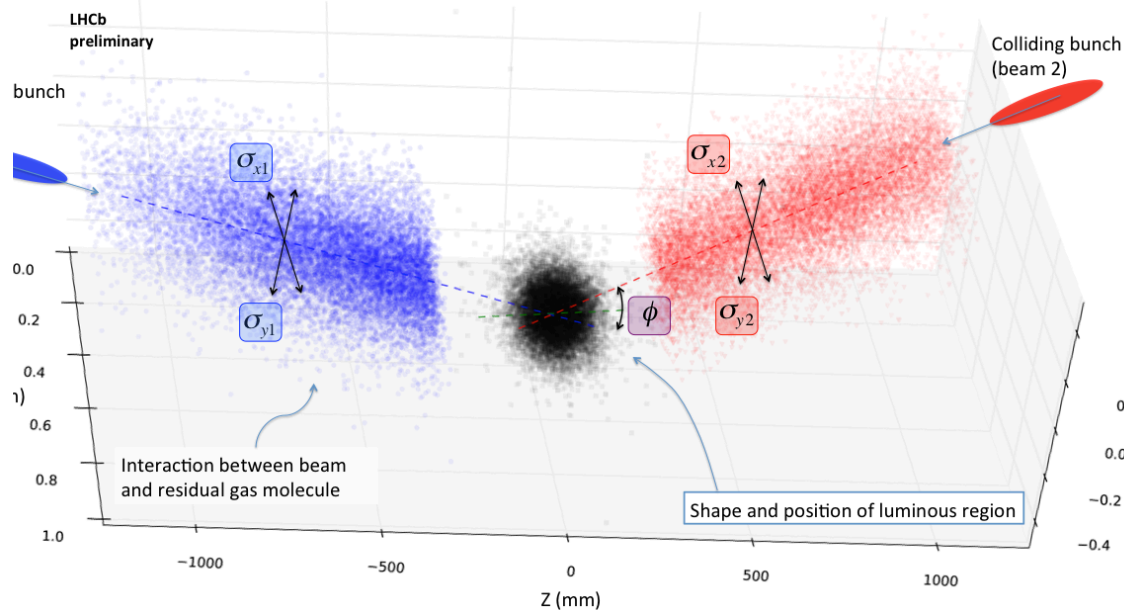
- Key assumption: **factorization** of luminosity profile

$$\mathcal{L}(\delta_x, \delta_y) = f_x(\delta_x) f_y(\delta_y)$$

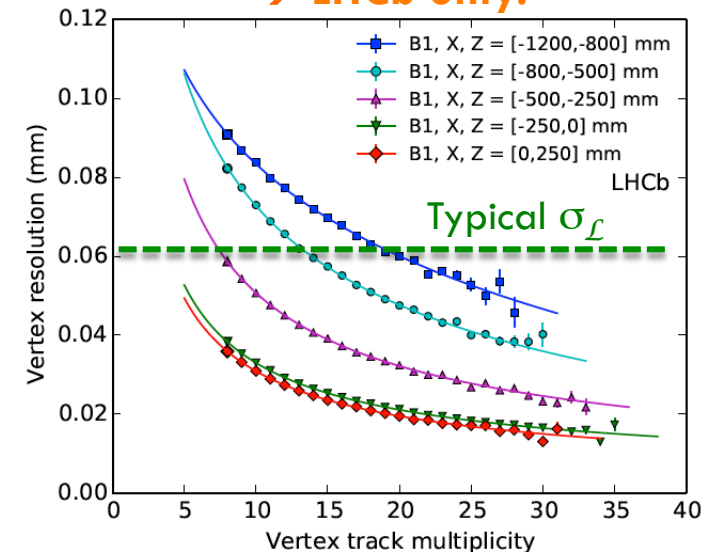
\mathcal{L} calibration: beam-gas imaging (BGI)

17

- Extract p -density distributions $\rho_{1,2}(x, y, z)$ from simultaneous fit to 3D distributions of B1-gas, B2-gas & pp collision vertices
- Each beam modelled by non-factorizable sum of 3D gaussians
- $\mathcal{L} = 2c f_r n_1 n_2 \cos \phi/2 \int \rho_1(x, y, z, t) \rho_2(x, y, z, t) dx dy dz dt$



Most critical:
vertexing resolution
→ LHCb only!



\mathcal{L} calibration: lessons from LHC run 1

18

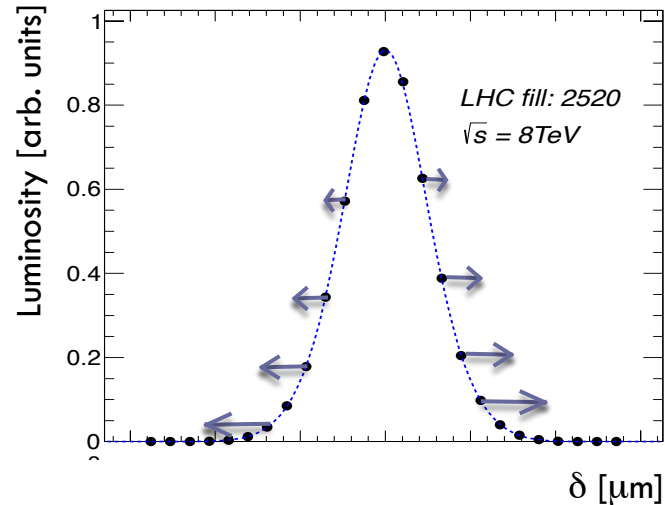
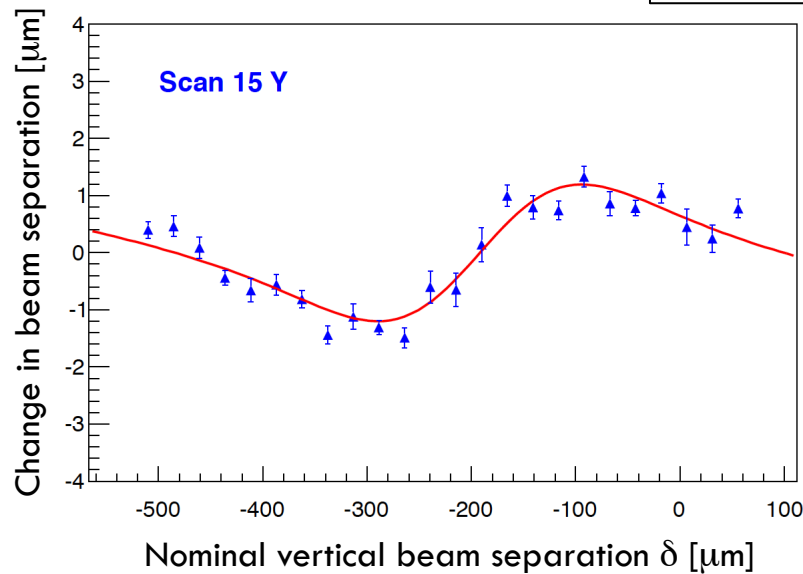
- The central role of **beam dynamics**
 - \mathcal{L} calibs: widely-spaced low- l bunches, no high- μ trains!
 - injected-beam quality, parasitic beam-beam, μ -dependence
 - orbit drifts can cost 2-3% of bias &/or systematics
 - **beam-beam** deflections & dyn. β **must be corrected for**
 - **non-factorization** an **often dominant** uncertainty
- Luminosity **instrumentation: redundancy** essential!
 - non-linear headaches: μ -dep., but also total- \mathcal{L} dep.?
 - the pains of aging: **response drifts \leftrightarrow reproducibility**
 - Run 2 harder: 25 vs 50 ns, higher \mathcal{L} / multiplicity / \int dose

Beam-beam corrections (1)

19

- Two distinct beam-beam effects: **beam-beam deflection** and dynamic β
 - ▣ bias σ_{vis} if not corrected
 - ▣ $< 0.5\%$ PbPb, 1 - 2% for 7/8/13 TeV pp and around 4% for 5 TeV pp
 - ▣ The interaction of the two beams during a scan causes **distortion to the scan curve**

Beam-beam deflection



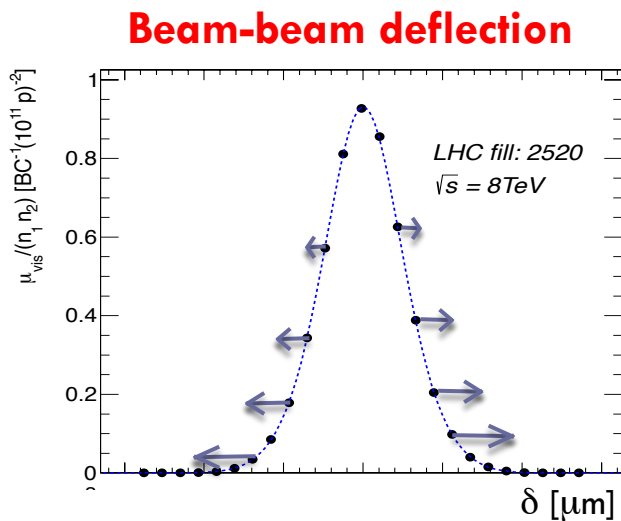
(Size of effect exaggerated for demonstration)

True beam separation larger than nominal separation δ

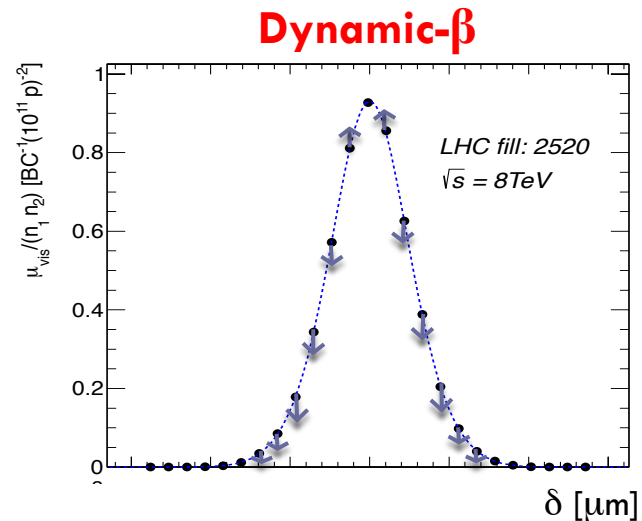
Beam-beam corrections (2)

20

- Two distinct beam-beam effects: **beam-beam deflection** and **dynamic β**
 - ▣ bias σ_{vis} if not corrected
 - ▣ **< 0.5% PbPb, 1 - 2% for 7/8/13 TeV pp** and around **4% for 5 TeV pp**
 - ▣ The interaction of the two beams during a scan causes **distortion to the scan curve**



True beam separation larger than nominal separation δ



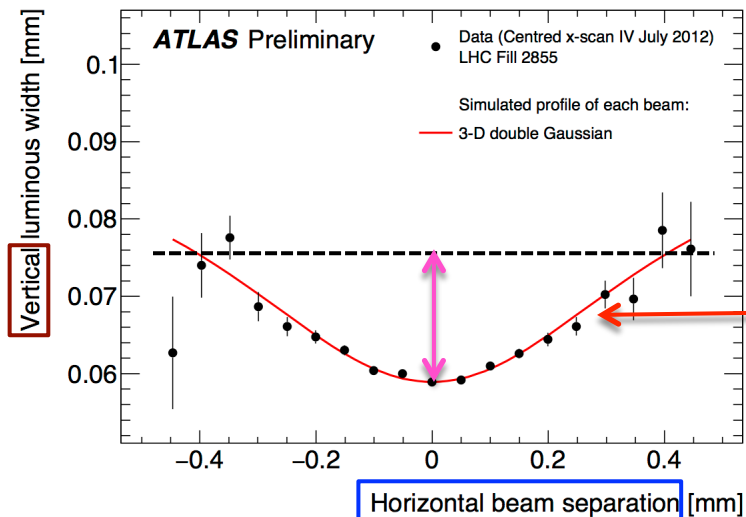
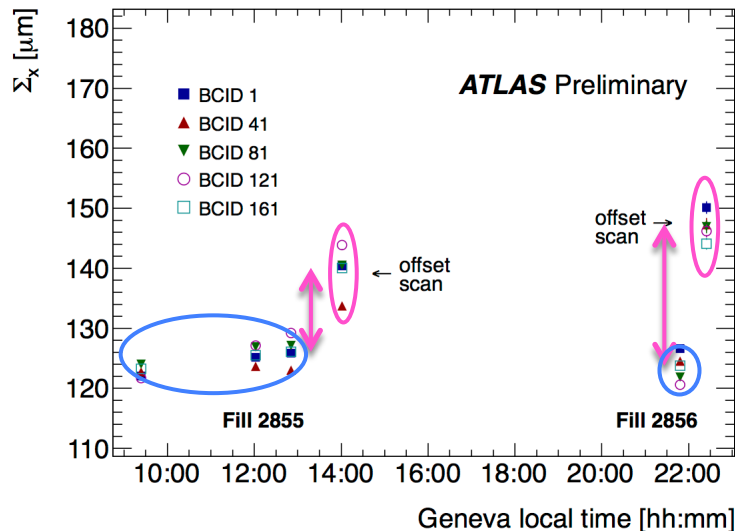
Beams focus/defocus each other by an amount that is a function of separation

(Size of effects exaggerated for demonstration)

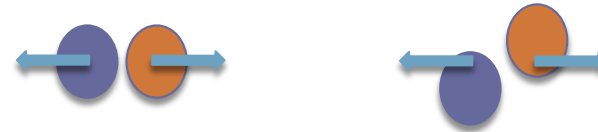
$$\mathcal{L}(\delta_x, \delta_y) = f_x(\delta_x) f_y(\delta_y) ?$$

Evidence for non-factorization

21



□ $\Sigma_{x,y}$ in **on-axis** vs. **off-axis** scans

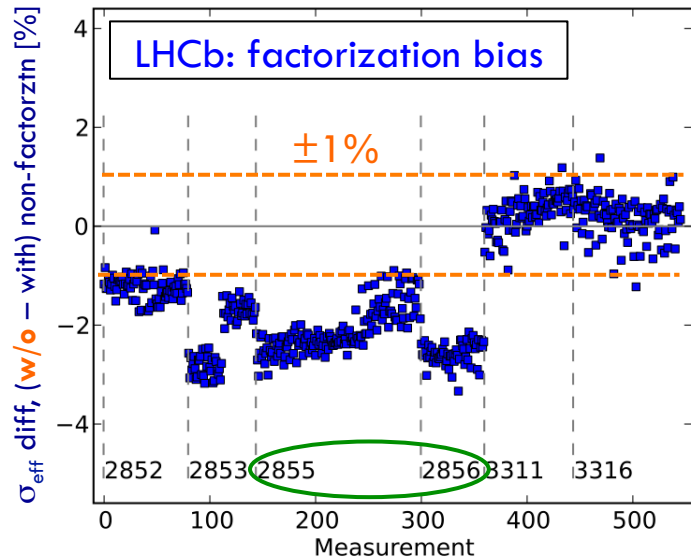


- Σ_x, Σ_y in **offset** scans **larger** than **on-axis** [in this example: **10-20%**]
- varies from fill to fill
- → **empirical tailoring of beams** in injectors
- $\sigma_{\mathcal{L},xy}$ (x, y luminous size) in on-axis scans
 - **Vertical** luminous width depends on **horizontal** separation (and vice-versa) [in this example: **~20%**]
 - → **correct** using single-beam parameters from **combined fit** to beam-separation dependence of \mathcal{L} and of luminous-region observables: $\langle x, y, z \rangle_{\mathcal{L}}, \sigma_{x, y, z, \mathcal{L}}, \dots$

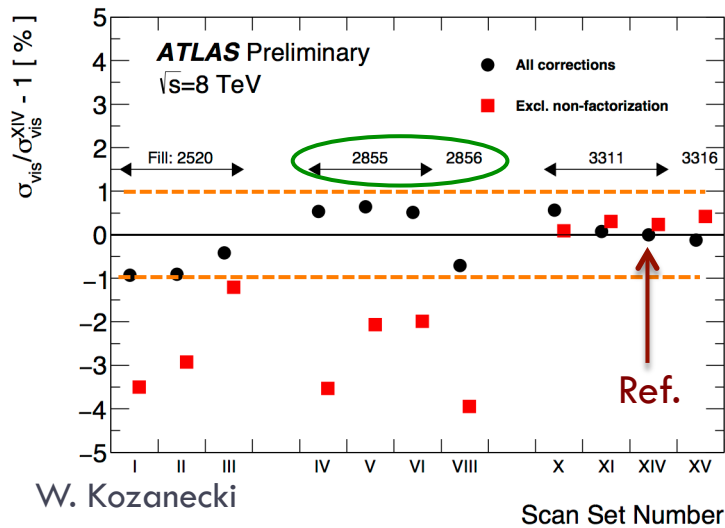
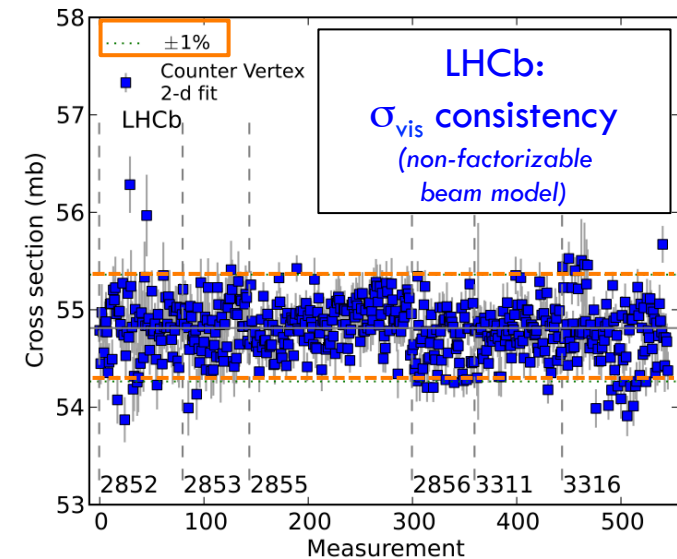
$$\mathcal{L}(\delta_x, \delta_y) \neq f_x(\delta_x) f_y(\delta_y) !$$

Non-factorization: impact

22



LHCb
beam imaging



ATLAS
vdM scans
without/with
non-factorization
correction

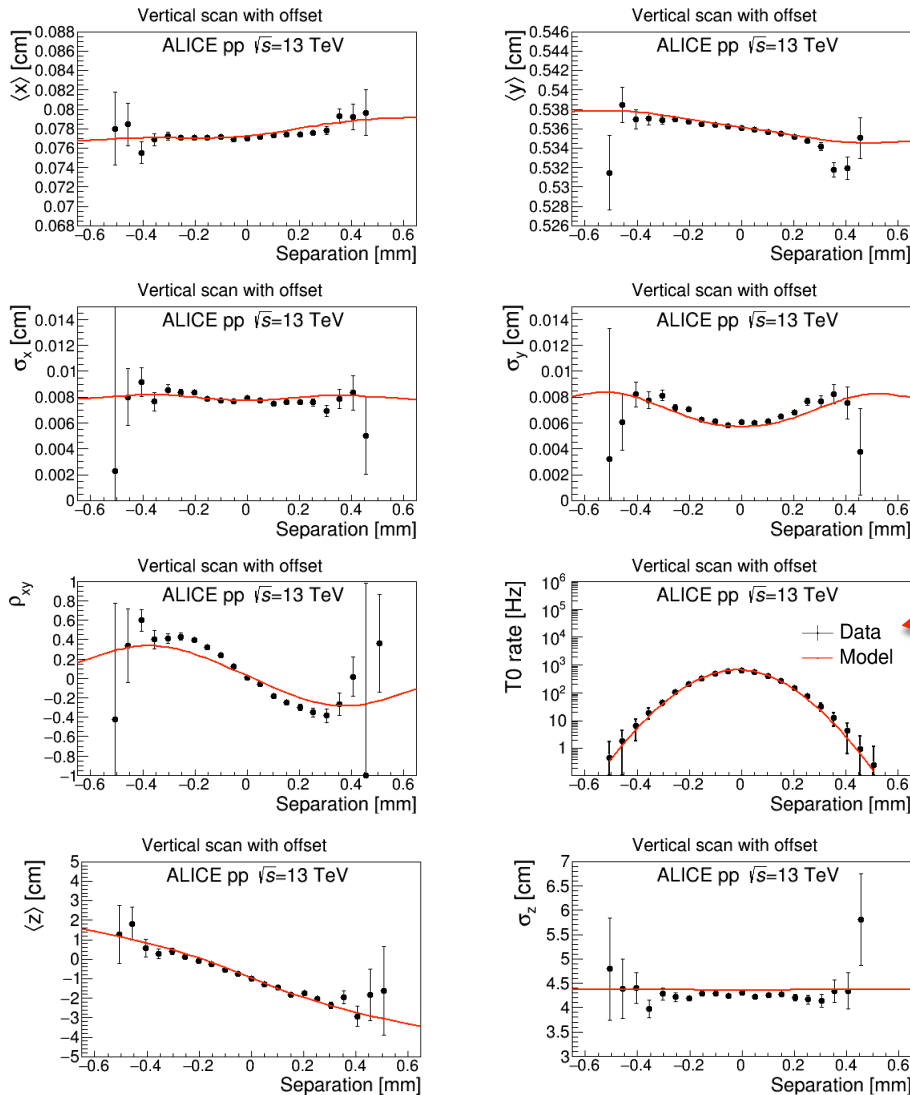
Magnitude of factorization bias:

- fill-dependent
- time-dependent within a fill

$$\mathcal{L}(\delta_x, \delta_y) \neq f_x(\delta_x) f_y(\delta_y) !$$

Non-factorization corrections

23



Accounting for non-factorization

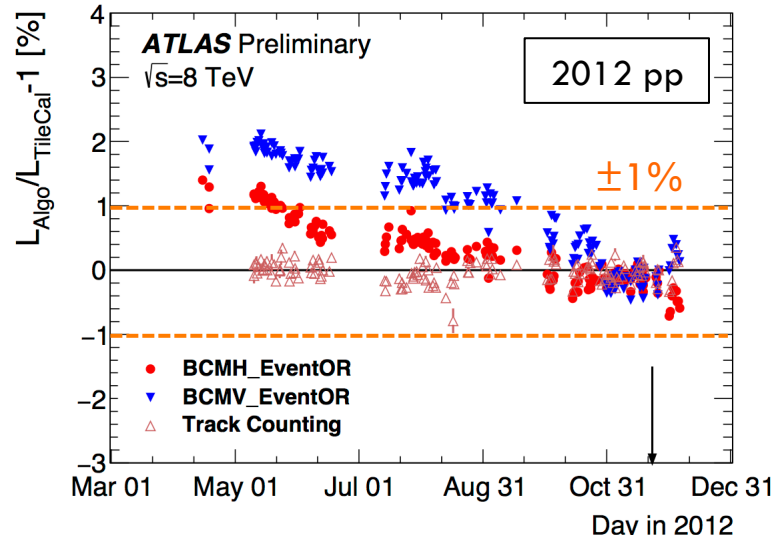
- Direct measurement: beam-gas imaging (LHCb)
- Factorizable (= “naive”) vdM analysis + non-factorization correction from spatial dependence of $N_{\text{vtx}}(x, y, z) [\sim \mathcal{L}(x, y, z)]$
 - luminous-region evolution analysis (ALICE, ATLAS)
 - beam-beam imaging (CMS)
- Non-factorizable vdM analysis (ALICE, ATLAS, CMS, LHCb)
 - coupled vdM fits to $\mathcal{L}(\delta_x), \mathcal{L}(\delta_y)$

Consistency btwn methods: fill-dependent

Associated systematic: 0.5 – 3%

Aging pains: a price to pay for high \mathcal{L}

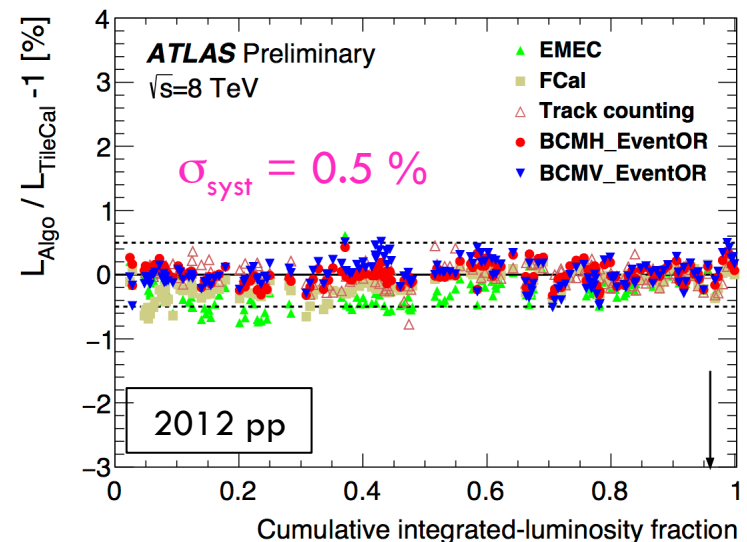
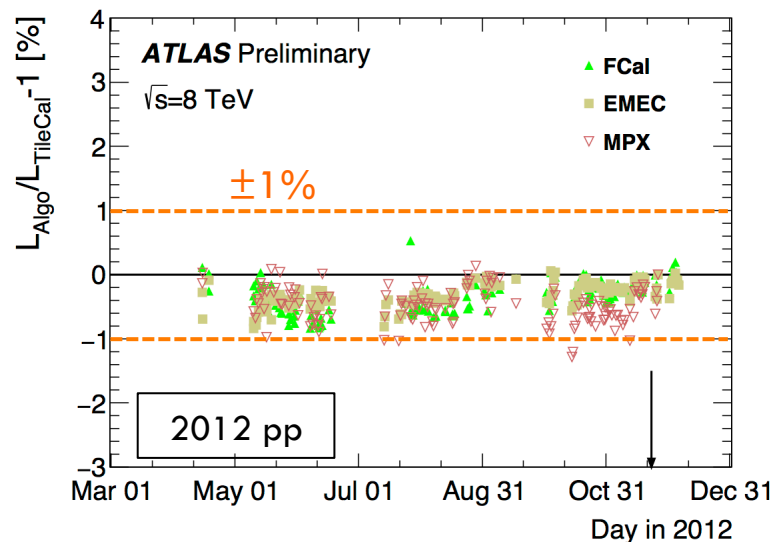
24



Long-term drift correction

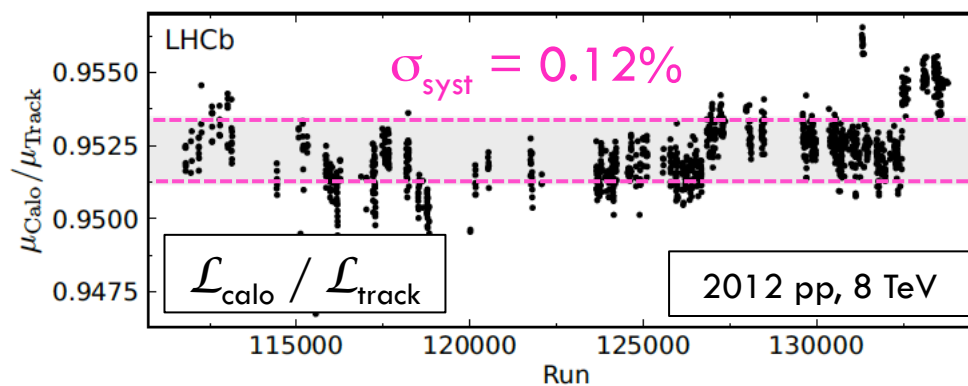
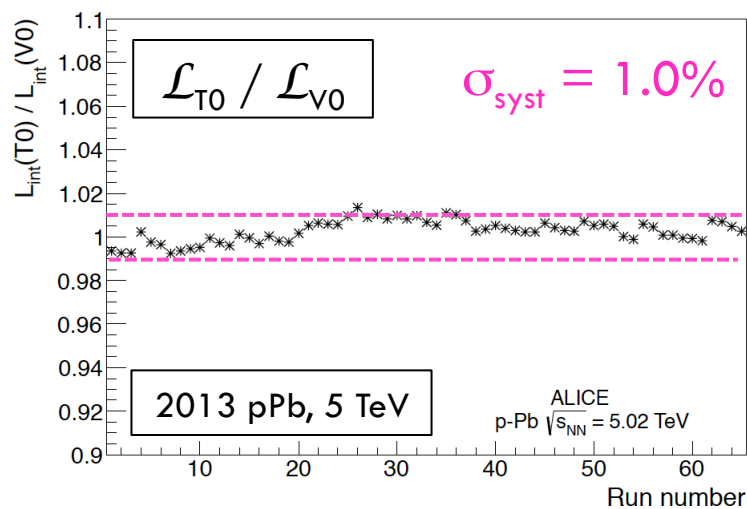
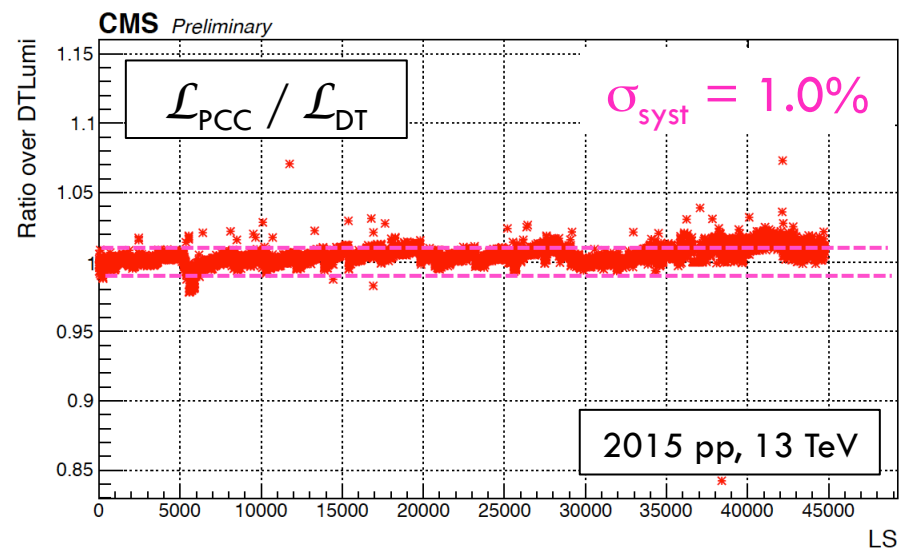
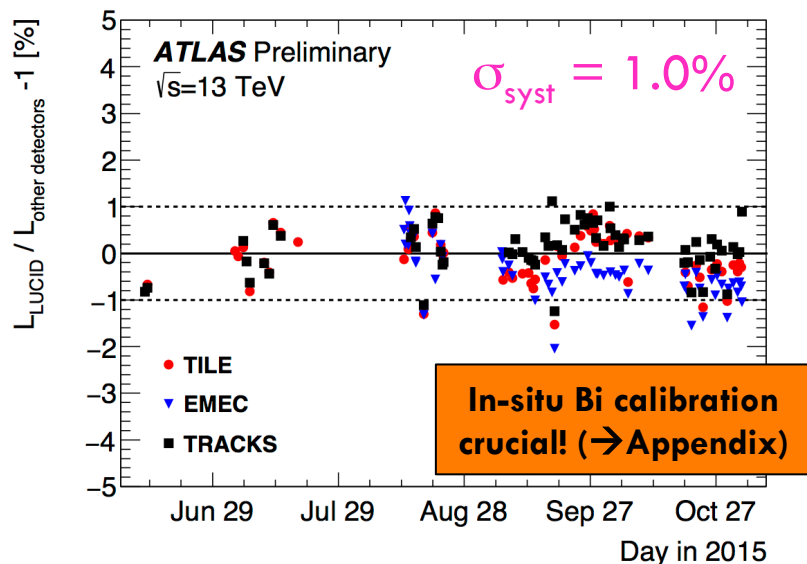
ATLAS (2012, 8 TeV pp):

- BCM (diamond) response degraded by $\sim 2\%$ over the year
- corrected using either calorimeter- or track-based \mathcal{L} (systematic: 0.3%)
- resulting relative stability $< 0.5\%$ across 5 independent luminometers



Long-term consistency of \mathcal{L} measurements

25



Total \mathcal{L} systematics: vdM or BGI - & more

26

Experiment <i>pp</i> running period \sqrt{s} (TeV)	ALICE 2010 7.0	ATLAS 2012 8.0	CMS 2012 8.0		LHCb 2012 8.0	
Absolute-calibration method	<i>vdM</i>	<i>vdM</i>	<i>vdM</i>	<i>vdM</i>	Combined	BGI
Calibration uncertainty $\Delta \sigma_{vis} / \sigma_{vis}$ (%)	3.5	1.2	2.3	1.47	1.12	1.43
μ or total-rate dependence (%)	-	1.4	< 0.1		0.17	
Long-term stability (%)	1.5	0.6	1.0		0.22	
Subtraction of luminosity backgrounds (%)	3.0	0.2	0.5		0.13	
Other luminosity-dependent effects (%)	1.5		0.5		-	
Total luminosity uncertainty (%)	5.0	1.9	2.6	1.5	1.2	1.5

Adapted from ref. [1], Table 14

\mathcal{L} performance summary

27

	LHCb	ATLAS	CMS	LHCb	ALICE	ATLAS	CMS	LHCb
Running period	2011 pp	2012 pp	2012 pp	2012 pp	2015 pp	2015 pp	2015 pp	2015 pp
\sqrt{s} [TeV]	7	8	8	8	5/13	13	13	13
$\sigma_{\mathcal{L}}/\mathcal{L}$ [%]	1.7	1.9	2.5	1.2	2.2/3.4	2.1	2.7 Prelim.	3.9 Prelim.

	ALICE	ALICE	ATLAS	CMS	LHCb	ATLAS	CMS	LHCb
Running period	2010/2011 PbPb	2013 p-Pb / Pb-p	2013 p-Pb / Pb-p	2013 p-Pb / Pb-p	2013 p-Pb / Pb-p	2013 pp	2015 pp	2013 pp
$\sqrt{s_{NN}}$ [TeV]	5	5	5	5	5	2.76	5.02	2.76
$\sigma_{\mathcal{L}}/\mathcal{L}$ [%]	5.8/4.2	3.7/3.4	2.7	3.6/3.4	2.3/2.5	3.1	2.3	2.2

Why does $\sigma^{\text{syst}}_{\mathcal{L}}$ matter? some examples...

28

	Physics measurement	$\sqrt{s_{\text{NN}}}$ [TeV]	$\sigma^{\text{syst}}_{\text{tot}}$ [%]	$\sigma^{\text{syst}}_{\mathcal{L}}$ [%]	Ref.
ALICE	Total inelastic pp cross-section	7	+4.5 -7.2	3.6	[13]
	EM dissociation cross section in Pb-Pb collisions	5	6.5	5.8	[3]
ATLAS	Top-quark pair production cross-section	7	3.5	2.0	[4]
	Fiducial inclusive $Z \rightarrow \mu\mu$ cross-section	7	1.85	1.80	[6]
	Top-quark pair production ratio, $\sigma_{8 \text{ TeV}} / \sigma_{7 \text{ TeV}}$	8/7	3.9	3.7	[4]
CMS	Top-quark pair production cross-section	13	5.5	2.6	[10]
	Fiducial inclusive Z cross-section	13	3.3	2.7	[11]
LHCb	Forward Z+jet production	8	4.8	1.2	[19]
	Prompt D0 production cross-section	13	5.3	3.9	[20]

Example of impact of $\sigma_{\mathcal{L}}$ on SM precision tests: W & Z fiducial cross-sections at 7 TeV

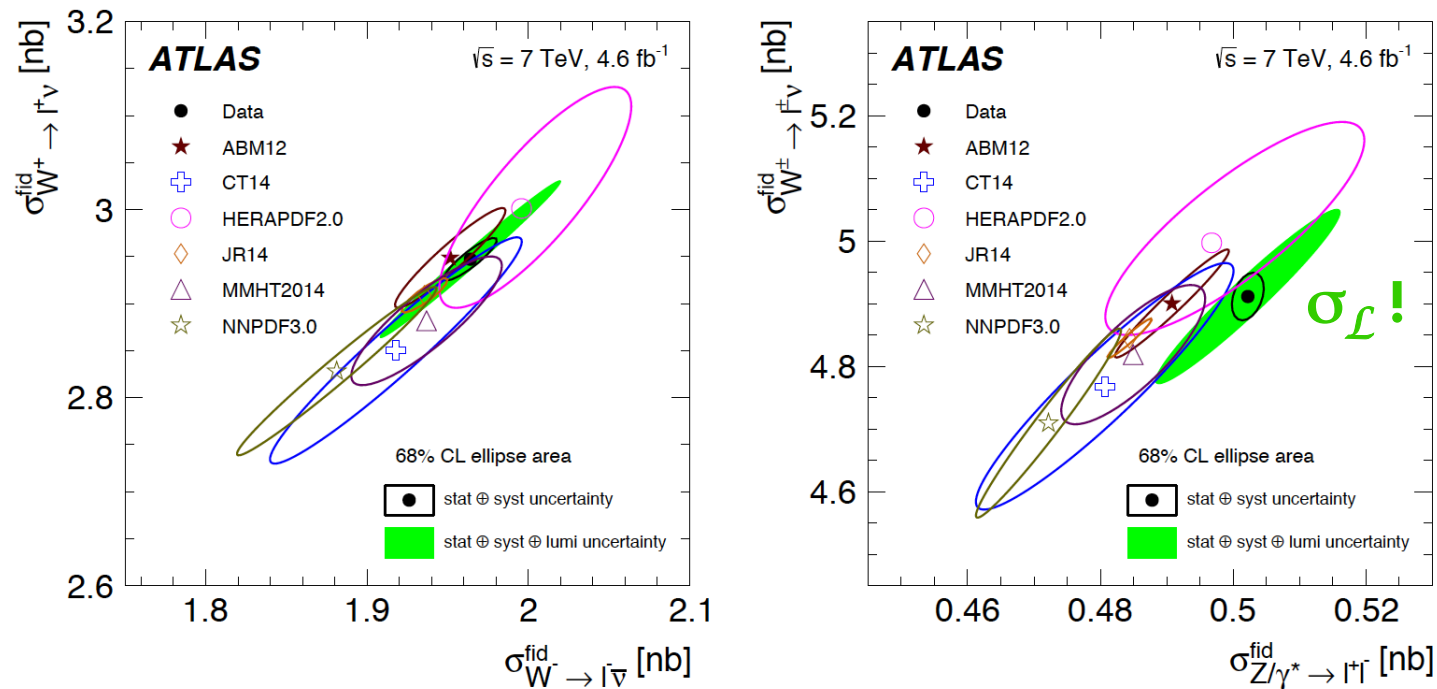


Figure 19: Integrated fiducial cross sections times leptonic branching ratios of $\sigma_{W^+ \rightarrow \ell^+ \nu}^{\text{fid}}$ vs. $\sigma_{W^- \rightarrow \ell^- \bar{\nu}}^{\text{fid}}$ (left) and $\sigma_{W^+ \rightarrow \ell^+ \nu}^{\text{fid}}$ vs. $\sigma_{Z/\gamma^* \rightarrow \ell^+ \ell^-}^{\text{fid}}$ (right). The data ellipses illustrate the 68% CL coverage for the total uncertainties (full green) and total excluding the luminosity uncertainty (open black). Theoretical predictions based on various PDF sets are shown with open symbols of different colours. The uncertainties of the theoretical calculations correspond to the PDF uncertainties only.

Example of impact of $\sigma_{\mathcal{L}}$ on SM precision tests: Z cross-sections ratios at 7, 8 & 13 TeV

30

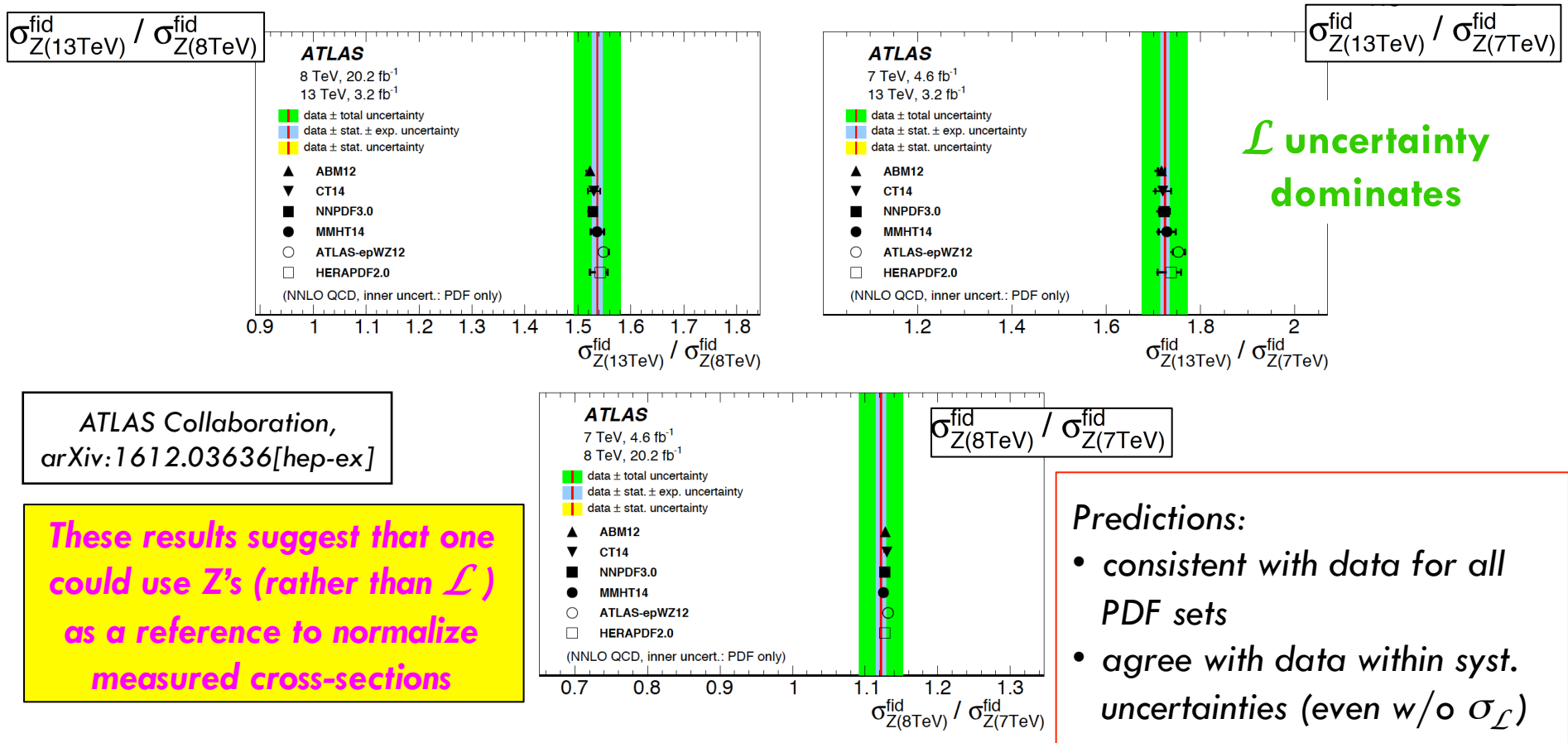


Figure 4: The ratios R_{Z_i/Z_j}^{fid} , for $i, j = 13, 8, 7$ compared to predictions based on different PDF sets. The inner shaded band (barely visible since it is small) corresponds to the statistical uncertainty, the middle band to the statistical and experimental systematic uncertainties added in quadrature, while the outer band shows the total uncertainty, including the luminosity uncertainty. The theory predictions are given with the corresponding PDF uncertainties shown as inner bars while the outer bars include all other uncertainties added in quadrature.

Example of impact of $\sigma_{\mathcal{L}}$ on SM precision tests: $t\bar{t}$ cross-sections ratios at 7, 8 & 13 TeV

31

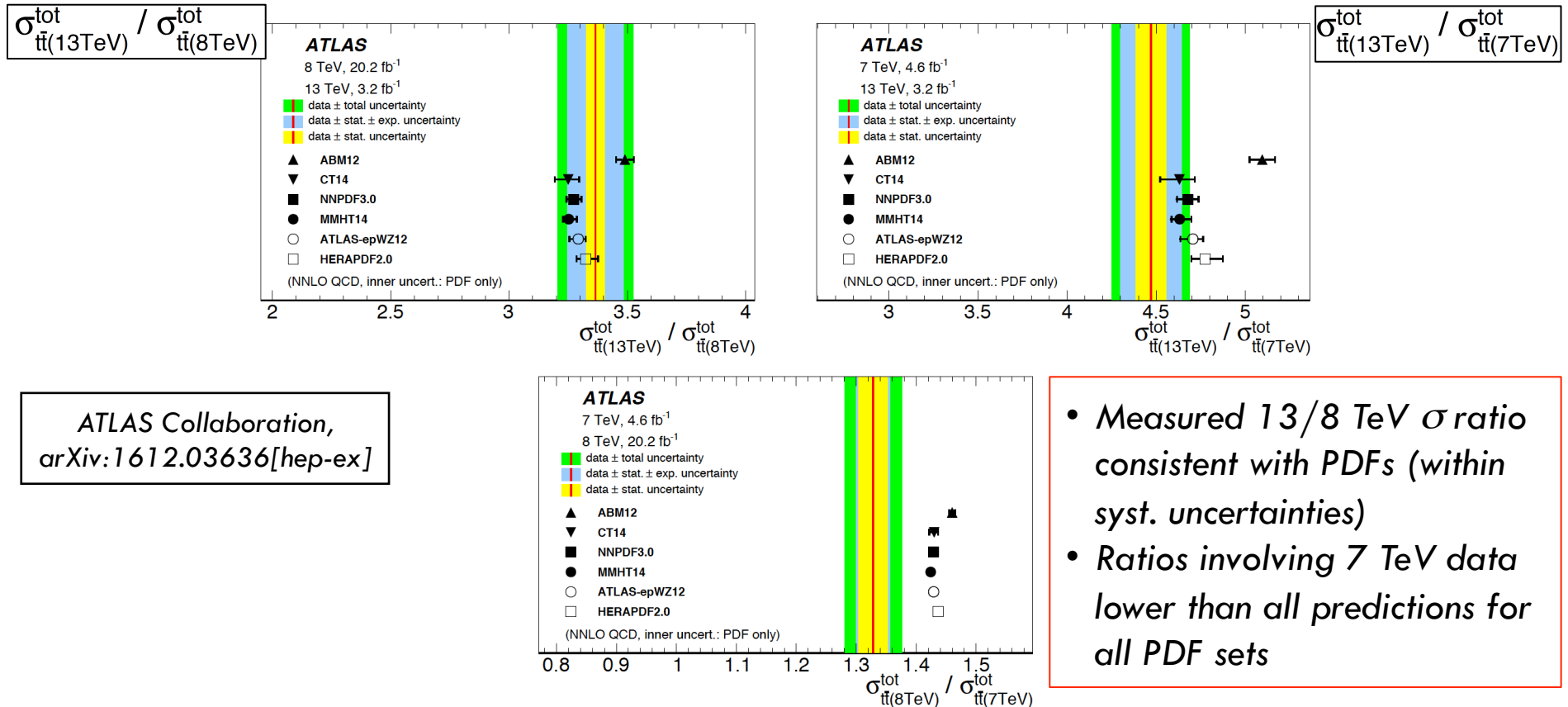


Figure 5: The ratios $R_{i\bar{i}/j\bar{j}}^{\text{tot}}$, for $i, j = 13, 8, 7$ compared to predictions based on different PDF sets. The inner shaded band corresponds to the statistical uncertainty, the middle band to the statistical and experimental systematic uncertainties added in quadrature, while the outer band shows the total uncertainty, including the luminosity uncertainty. For the 8-to-7 TeV ratio, the experimental systematic uncertainty band is too small to be clearly visible. The theory predictions are given with the corresponding PDF uncertainties shown as inner bars while the outer bars include all other uncertainties added in quadrature.

Conclusions

32

- The absolute precision of the integrated \mathcal{L} typically lies in the 2-3 % (3-6%) range for top-energy pp (HI)
 - ▣ main contributors to the uncertainty
 - beam dynamics: phase-space control (non-factorization, satellites, ghosts), beam-beam \leftrightarrow calibration strategy
 - instrumental linearity vs μ & \mathcal{L}_{tot} (4 orders of magnitude!)
 - instrumental stability & aging (more difficult for high- \mathcal{L} expts)
- Run 2 already is a challenge; HL-LHC is *Terra Incognita*
 - breaking the “2% wall” very challenging- except (?) for LHCb:
 - unique capability to combine vdM- & BGI-based calibrations
 - low- μ operating regime, dictated by specialized physics goals
 - HL-LHC: how can we fulfill the theorists’ hopes?

Selected bibliography: general

33

- Detailed experimental review of \mathcal{L} -determination methodology, from the ISR to the LHC

[1] P. Grafstrom & W. Kozanecki, *Luminosity determination at proton colliders*, *Progr. Nucl. Part. Phys.* 81 (2015) 97–148

- Precision goals at HL-LHC

[2] G. P. Salam, *Theoretical Perspective on SM and Higgs Physics at HL-LHC*, 2016 ECFA High-Luminosity LHC Experiments Workshop, <https://indico.cern.ch/event/524795/contributions/2235443/attachments/1347759/2034269/HL-LHC-SMHiggs-theory.pdf>

Selected bibliography: ATLAS

34

□ ATLAS Collaboration

- [3] *Improved luminosity determination in pp collisions at $\sqrt{s} = 7$ TeV using the ATLAS detector at the LHC*, Eur. Phys. J. C73 (2013) 2518
- [4] *Measurement of the $t\bar{t}$ production cross-section using $e\mu$ events with b -tagged jets in pp collisions at $\sqrt{s} = 7$ and 8 TeV with the ATLAS detector*, Eur. Phys. J. C74 (2014) 3109
- [5] *Luminosity determination in pp collisions at $\sqrt{s} = 8$ TeV using the ATLAS detector at the LHC*, Eur. Phys. J. C76 (2016) 653
- [6] *Precision measurement and interpretation of inclusive W^+ , W^- and Z/γ^* production cross sections with the ATLAS detector*, submitted to EPJC, arXiv:1612.03016[hep-ex]
- [7] *Measurements of top-quark pair to Z-boson cross-section ratios at $\sqrt{s} = 13, 8, 7$ TeV with the ATLAS detector*, submitted to JHEP, arXiv:1612.03636 [hep-ex]

Selected bibliography: CMS

35

□ CMS Collaboration

- [8] *CMS Luminosity Based on Pixel Cluster Counting - Summer 2013 Update*, CMS-PAS-LUM-13-001 (Sep. 2013)
- [9] *Luminosity Calibration for the 2013 Proton-Lead and Proton-Proton Data Taking*, CMS-PAS-LUM-13-002 (Jan 2014)
- [10] *Measurement of the top quark pair production cross section using $e\mu$ events in proton-proton collisions at $\sqrt{s} = 13$ TeV with the CMS detector*, CMS PAS TOP-16-005 (March 2016), submitted to EPJC
- [11] *Measurements of inclusive and differential Z boson production cross sections in pp collisions at $\sqrt{s} = 13$ TeV*, CMS PAS SMP-15-011 (March 2016)
- [12] *CMS Luminosity Measurement for the 2015 Data Taking Period*, CMS-PAS-LUM-15-001 (March 2016)

Selected bibliography: ALICE

36

□ ALICE Collaboration

- [13] *Measurement of inelastic, single- and double-diffraction cross sections in proton–proton collisions at the LHC with ALICE,*
Eur. Phys. J. C73 (2013) 2456
- [14] *Performance of the ALICE Experiment at the CERN LHC,*
Int. J. Mod. Phys. A 29 (2014) 1430044
- [15] *Measurement of the Cross Section for Electromagnetic Dissociation with Neutron Emission in Pb-Pb Collisions at $\sqrt{s_{NN}} = 2.76$ TeV,*
PRL 109, 252302 (2012)
- [16] *Measurement of visible cross sections in proton-lead collisions at $\sqrt{s_{NN}} = 5.02$ TeV in van der Meer scans with the ALICE detector,*
JINST 9 (2014) 1100
- [17] *ALICE luminosity determination for pp collisions at $\sqrt{s} = 13$ TeV,*
ALICE-PUBLIC-2016-002

Selected bibliography: LHCb

37

□ LHCb Collaboration

[18] *Precision luminosity measurements at LHCb*, JINST 9 (2014) P12005

[19] *Measurement of forward W and Z boson production in association with jets in proton-proton collisions at $\sqrt{s} = 8$ TeV*, JHEP 05 (2016) 131

[20] *Measurements of prompt charm production cross-sections in pp collisions at $\sqrt{s} = 13$ TeV*, JHEP 03 (2016) 159

2017 planning: scenarios

38

40 - 45 fb⁻¹ ?

Parameter	Standard	BCMS 25 ns	BCMS 25 ns (pushed)
Beam energy [TeV]	6.5	6.5	6.5
β^* [cm]	40	40	33
Half crossing angle [μ rad]	185	155	170
Number of colliding bunches	2736	2448	2448
Protons per bunch [10^{11}]	1.25	1.25	1.25
Emittance into SB [μ m-rad]	3.2	2.3	2.3
Bunch length [ns, 4σ]	1.05	1.05	1.05
Peak luminosity [10^{34} cm ⁻² s ⁻¹]	1.4	1.7	1.9
Peak (average) mean pile-up	37 (27)	51 (33)	56 (36)
\mathcal{L} lifetime (burn-off only) [h]	21	15	14

39

Supplementary Material

ALICE luminometers for pp collisions

- **V0**

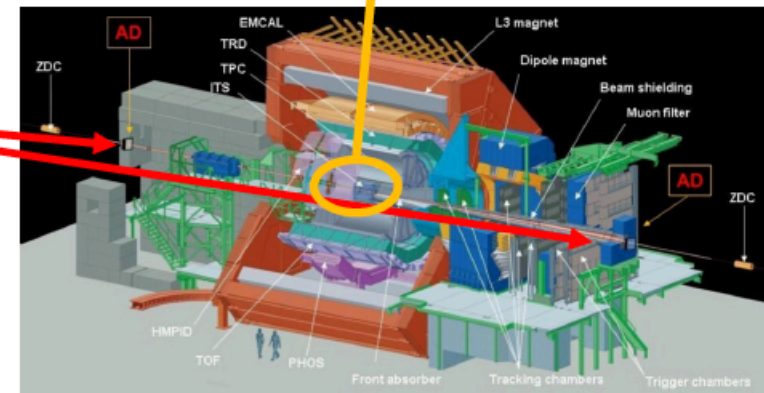
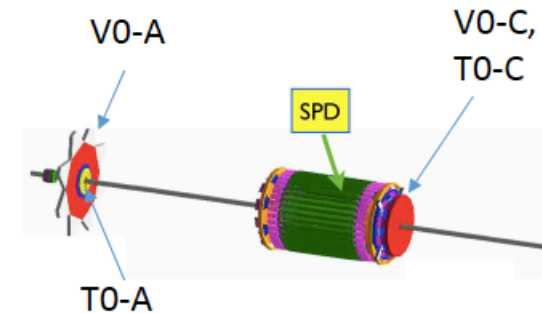
- two **scintillator** arrays on opposite side (A and C) of the IP ($2.8 < \eta < 5.1$; $-3.7 < \eta < -1.7$)
- coincidence of A and C side

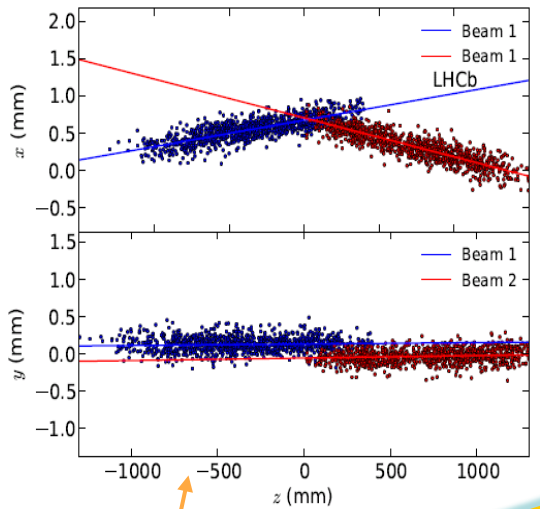
- **T0**

- two **Cherenkov** detector arrays on opposite sides of the IP ($4.61 < \eta < 4.92$; $-3.28 < \eta < -2.97$)
- coincidence of A and C side with hardware cut on the signal arrival time difference

- **AD (ALICE Diffractive)** → new wrt Run1

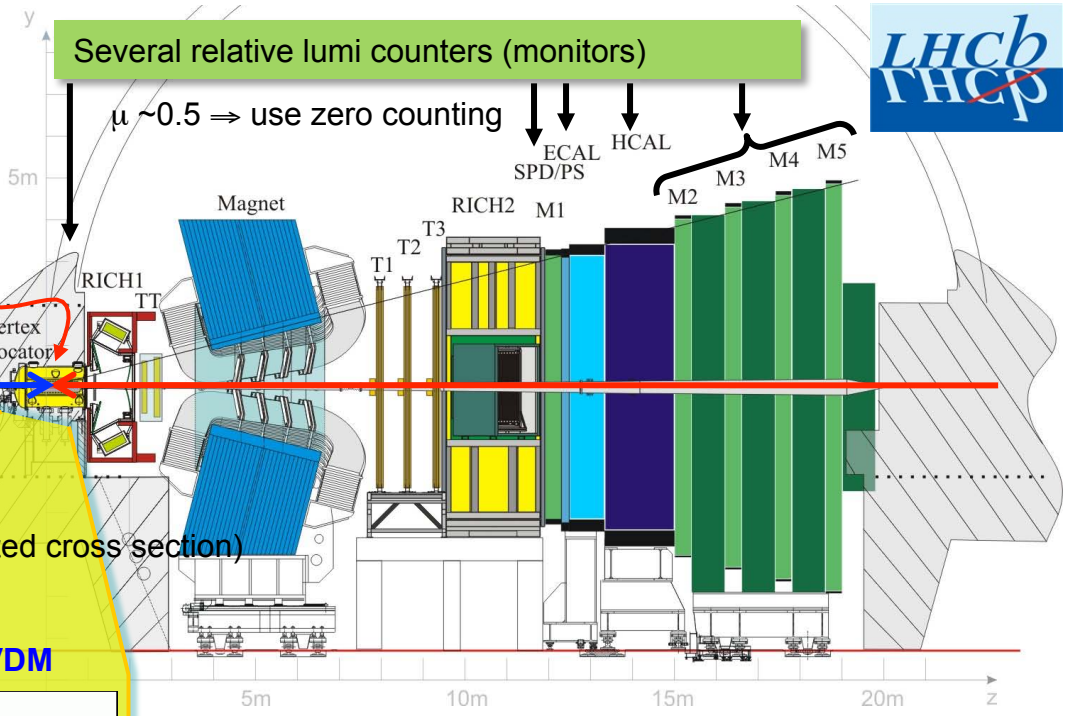
- two scintillator arrays on opposite side (A and C) of the IP ($4.8 < \eta < 6.3$; $-7 < \eta < -4.9$)
- coincidence of A and C side





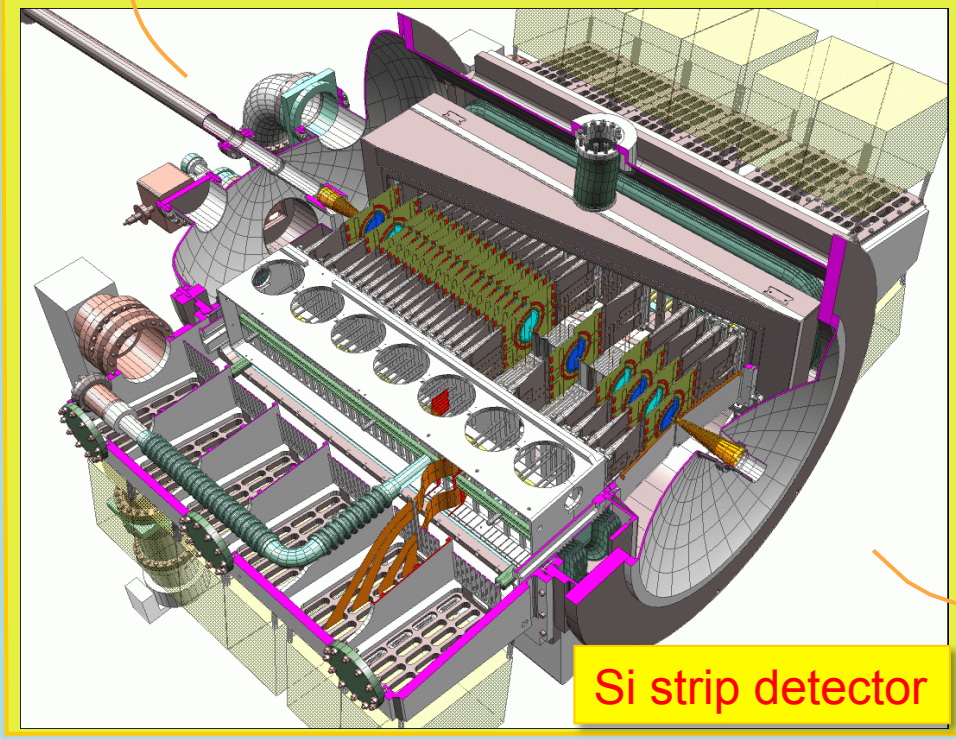
S ystem for
M easuring the
O verlap with
G as

Gas
injected
into beam
pipe



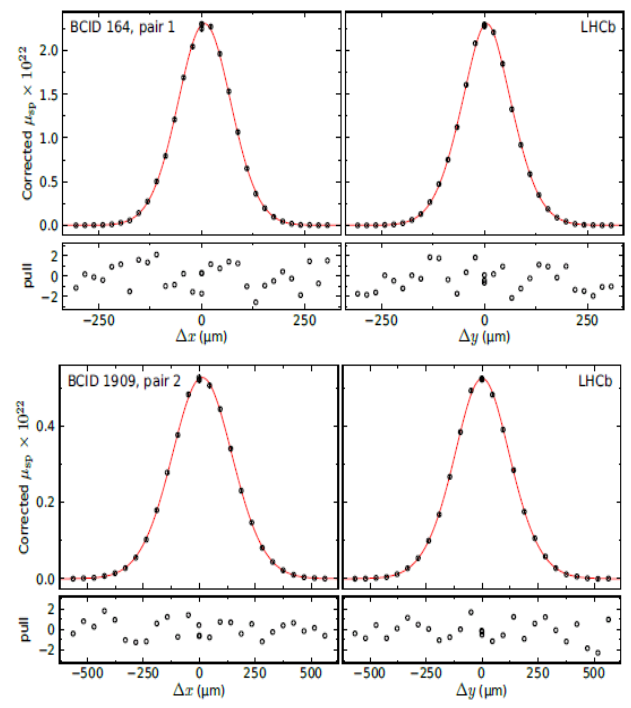
Beam
Gas
Imaging

- Our main detector for σ_{ref} (calibrated cross section)
 - Vtx counter
 - Track counter
- Two calibration methods: **BGI & VDM**



Si strip detector

Van der
Meer
scans



$$\mathcal{L}(\delta_x, \delta_y) = f_x(\delta_x) f_y(\delta_y) ?$$

Non-factorisation correction procedure

42

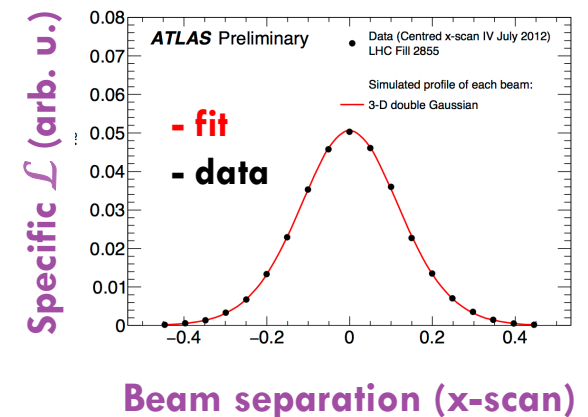
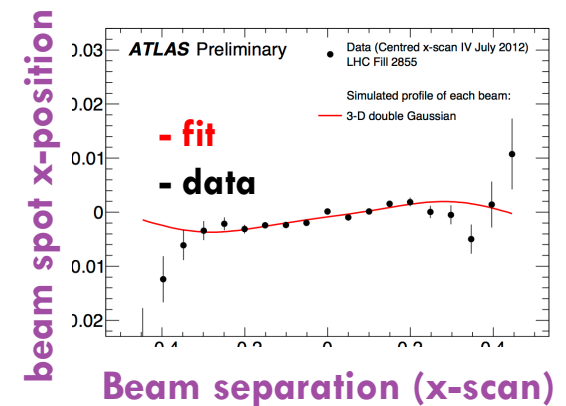
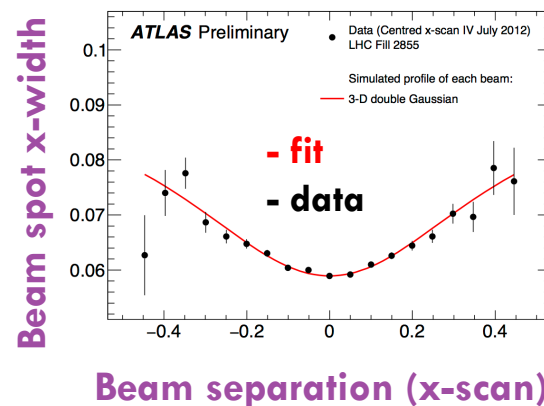
- Single beam profiles are parameterised by fitting the beam-separation dependence of the luminosity & of the beamspot displacement and width during a vdM scan.

This allows to:

- estimate the true luminosity (i.e. **unbiased by non-factorisation effects**)
- estimate **correction for non-factorisation, R** , with an associated uncertainty

$$R = \frac{\mathcal{L} \text{ not assuming factorisation}}{\mathcal{L} \text{ assuming factorisation}}$$

- The [ATLAS/ALICE] procedure above is closely related to the “beam-beam imaging” scans [pioneered by LHCb & recently tried by CMS] in which one beam is scanned transversely as a probe across the other.



Non-factorization correction: beam-beam imaging

43

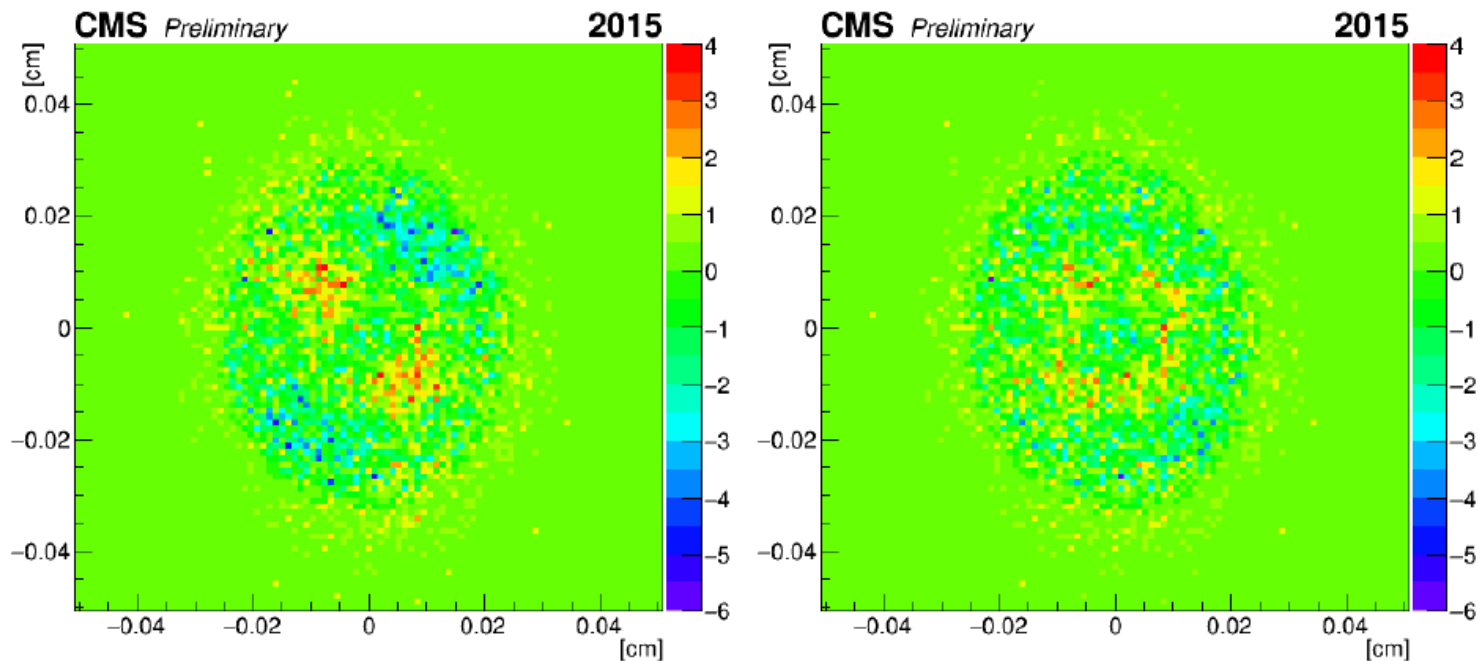
- Principle: use one beam (\sim wire) to probe the other
 - ▣ keep witness beam (B1) stationary; scan probe beam (B2) across it in x , then in y ; repeat with $B1 \leftrightarrow B2$
 - measure 2-d distribution of reco'd evt vertices at each step:
$$N_{\text{vtx}}(x, y) = \{\rho_{\text{witness}}(x, y) \times \rho_{\text{probe}}(x, y)\} \times R_{\text{vtx position}}(x, y)$$

(see ArXiv_1603.0356 [hep-ex])
 - ▣ extract single-beam parameters of B1 & B2 from fit to 2-d vertex distributions in the 4 scans (B1 / B2, x/y)
 - ▣ closely related to the ATLAS & ALICE luminous-region evolution method (but uses only transverse info, not \mathcal{L}/z)
 - common key issue: vertex-position resolution $R_{\text{vtx position}}$
 - pros & cons of the 2 approaches to be clarified

Non-factorization correction: beam-beam imaging (2)

44

Pull distribution to cumulative event-vertex distributions for 2 single-beam models:
factorizable non-factorizable

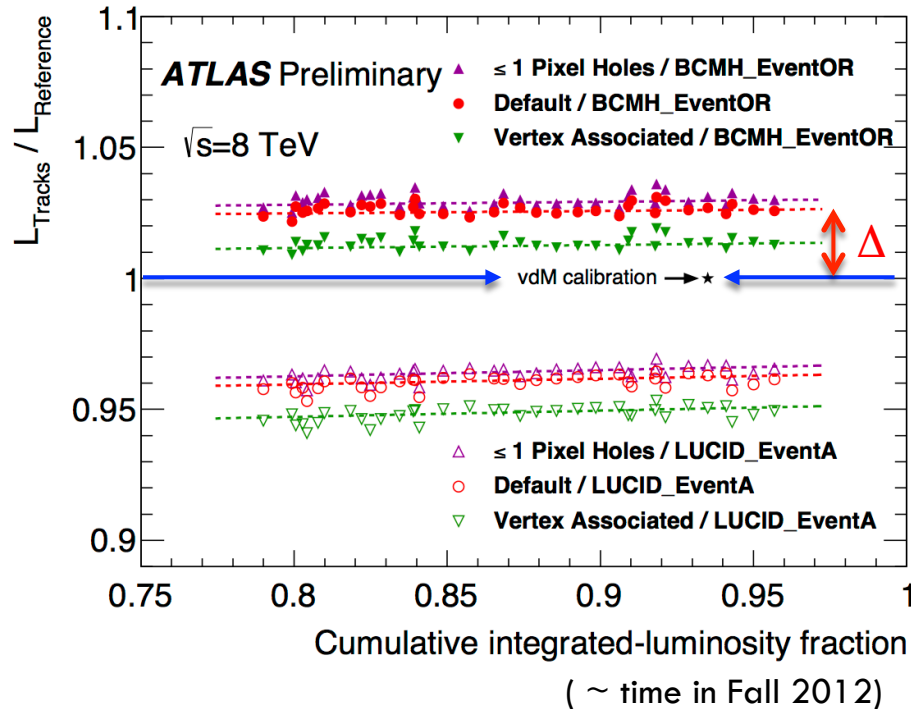


Example of pull distributions of the fitted single-beam model of the single-gaussian (factorizable, left) and double-gaussian (non-factorizable, right) type to the vertex distribution accumulated during scan Y3 of bunch pair 1631.

(Caption adapted from Fig. 11 of CMS-PAS-LUM-2015-001)

Beam-conditions-dependent biases

45



Calibration-transfer correction

ATLAS (2012 & 2015):

- luminometer response shifts by $\Delta = 2-4\%$ between vdM (low \mathcal{L} , bunches far apart) and physics (high \mathcal{L} , 50 or 25 ns trains)
- magnitude & sign \neq for diamond- & PMT-based luminometers
- track-counting & calo-based \mathcal{L} crucial to “transfer” calibration vdM \rightarrow high \mathcal{L}
- associated systematic: **1.4 %** (0.9%) for **8 TeV pp [2012]** (**13 TeV pp [2015]**)

CMS (2012 & 2015)

- qualitatively similar effects seen in CMS diamond detector – but no visible impact bec. main luminometer = Si pixel detector

ALICE & LHCb: lower μ , \mathcal{L} - less of an issue

vdM-calibration systematics: pp examples

46

Example breakdowns of the fractional systematic uncertainties affecting the determination of the visible pp cross-section σ_{vis} by the vdM method at the LHC.

Blank entries correspond to cases where the uncertainty is either not applicable to that particular experiment or scan session, is considered negligible by the authors, or is not mentioned in the listed reference.

Source: Progr. Nucl. Part. Phys. 81 (2015) 97–148, Table 12

Experiment Reference	ALICE [118]	ATLAS [26]	CMS [133]	LHCb [127]
<i>pp</i> running period	2011	2011	2012	2012
\sqrt{s} (TeV)	2.76	7.0	8.0	8.0
Total beam intensity	0.34%	0.23%	0.3%	0.23%
Bunch-to-bunch fraction	0.08%	0.20%	–	0.10%
Ghost charge and satellite bunches	0.45%	0.44%	0.2%	0.23%
Subtotal, bunch-population product	0.57%	0.54%	0.4%	0.34%
Orbit drift & beam-position jitter	–	0.32%	0.1%	0.32%
Bunch-to-bunch σ_{vis} consistency	–	0.55%	–	–
Emittance growth & scan-to-scan reproducibility	0.64%	0.67%	0.2%	0.80%
Dynamic β & beam–beam deflections	0.40%	0.50%	0.7%	0.28%
vdM fit model	–	0.28%	2.0%	0.54%
Non-factorization effects	0.60%	0.50%	in fit model	0.80%
Subtraction of luminosity backgrounds	0.30%	0.31%	–	0.14%
Subtotal, beam conditions	1.01%	1.24%	2.2%	1.33%
Difference of reference $\mathcal{L}_{\text{spec}}$ across luminometers	–	0.29%	–	–
μ -dependent non-linearities during vdM scans	–	0.50%	–	–
Other instrumental effects	0.20%	–	–	0.09%
Statistical uncertainty	–	0.04%	0.5%	0.04%
Subtotal, instrumental effects	0.20%	0.58%	0.5%	0.10%
Absolute beam-separation scale	1.41%	0.42%	0.5%	0.50%
Total systematic uncertainty on σ_{vis}	1.84%	1.53%	2.3%	1.47%

BGI-calibration systematics: example

47

Source of uncertainty	Uncertainty (%)	Correlated with vdM
Bunch-population product	0.23	Yes
Vertexing resolution: beam-beam events	0.93	No
Vertexing resolution: beam-gas events	0.55	No
Detector alignment & crossing angle	0.45	No
VELO transverse scale	0.05	Yes
Bunch-shape model	0.50	Yes
Longitudinal reconstruction efficiency	0.04	Yes
Pressure gradient	0.03	No
Convolved bunch length	0.05	No
Background subtraction (“Vertex” algorithm)	0.20	Yes
Bunch-to-bunch & fill-to-fill σ_{vis} consistency	0.54	No
Calibration transfer to “Tracks” algorithm	0.20	No
Statistical uncertainty	0.01	No
Total systematic uncertainty on σ_{vis}	1.43	

Systematic uncertainties affecting the LHCb absolute luminosity calibration by the BGI method at $\sqrt{s} = 8$ TeV [31,127].

Source: Progr. Nucl. Part. Phys. 81 (2015) 97–148, Table 13

vdM-calibration systematics: pPb example

48

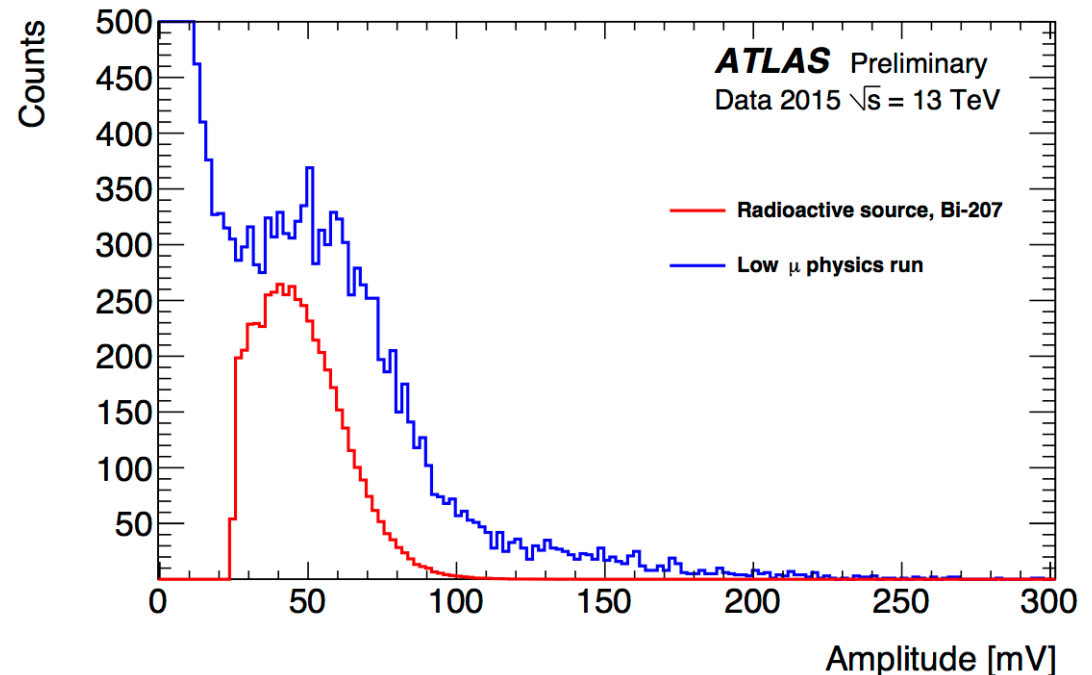
Uncertainty	p-Pp	Pb-p	Correlated between p-Pb and Pb-p
Transverse correlations	2.6%	2.3%	No
Bunch-by-bunch consistency	1.6%	-	No
Scan-to-scan consistency	0.5%	1.5%	No
Length-scale calibration	1.5%	1.5%	Yes
Background subtraction (V0 only)	0.5%	0.5%	Yes
Method dependence	0.3%	0.3%	No
Beam centering	0.3%	0.2%	No
Bunch size vs trigger	0.2%	0.2%	No
Bunch intensity	0.5%	0.5%	No
Orbit drift	0.4%	0.1%	No
Beam-beam deflection	0.2%	0.3%	Partially
Ghost charge	0.1%	0.2%	No
Satellite charge	<0.1%	0.1%	No
Dynamic β^*	<0.1%	0.1%	Partially
Total on visible cross section	3.5%	3.2%	
V0- vs T0-based integrated luminosity	1%	1%	No
Total on integrated luminosity	3.7%	3.4%	

Source: ALICE Collaboration, JINST 9 (2014) 1100, Table 3

LUCID-2 calibration using ^{207}Bi source

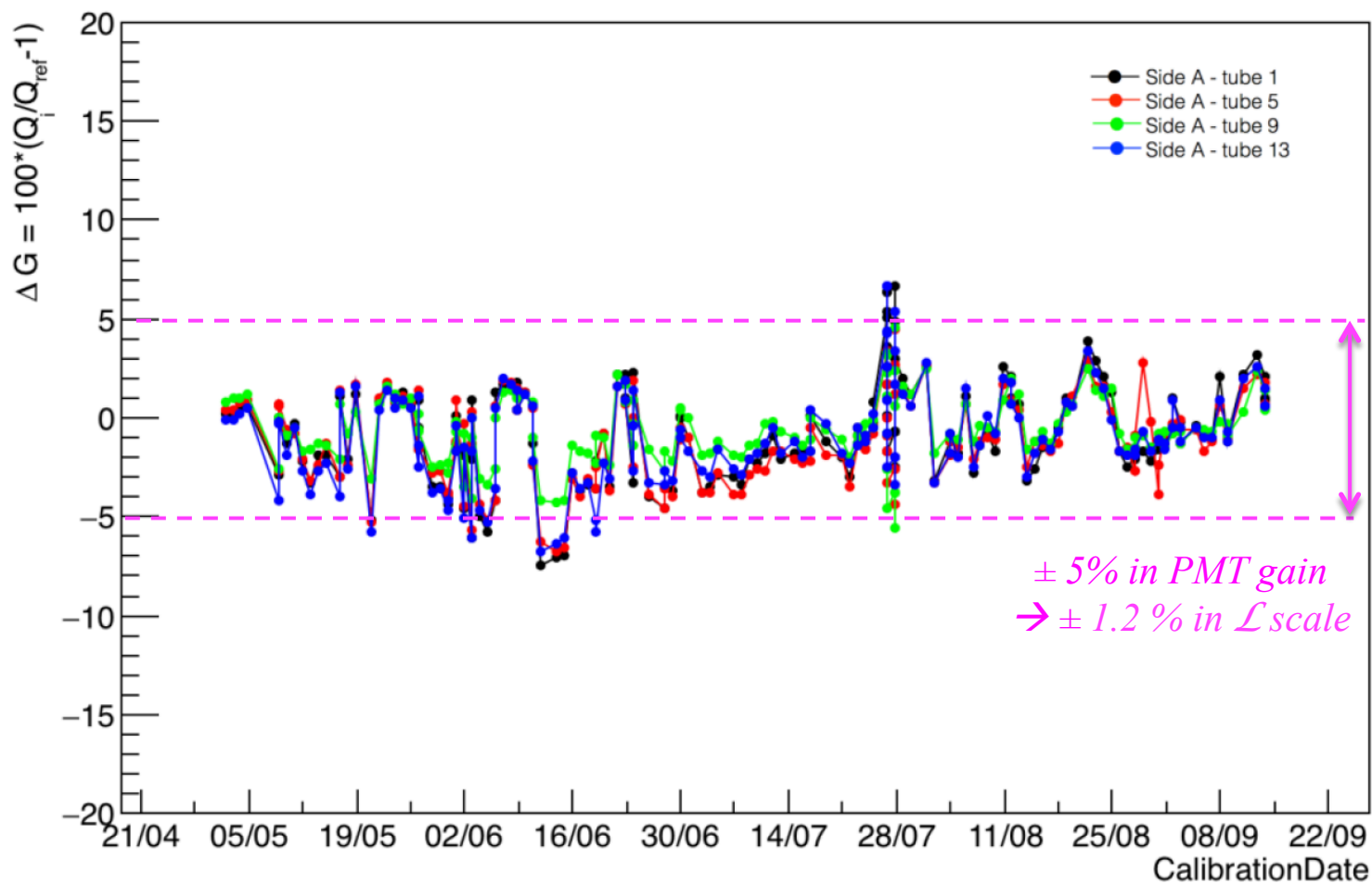
49

Pulse-height distributions from a LUCID photomultiplier recorded in 13 TeV runs on June 11 and 13, 2015 (blue) and in a calibration run recorded on June 25, 2015 (red). The physics runs were recorded using a random trigger, while the calibration run imposed a trigger-threshold requirement. The position of the peak created by Cherenkov photons produced in the quartz window of the photomultipliers is similar for high-energy particles from LHC collisions and low-energy electrons from the Bi-207 source. The vertical scale is set by the statistics of the low- μ run which has the smallest number of counts. The Bi-207 distribution has been arbitrary scaled down to a similar level.



ATLAS: LUCID-2 Bi-calibration stability

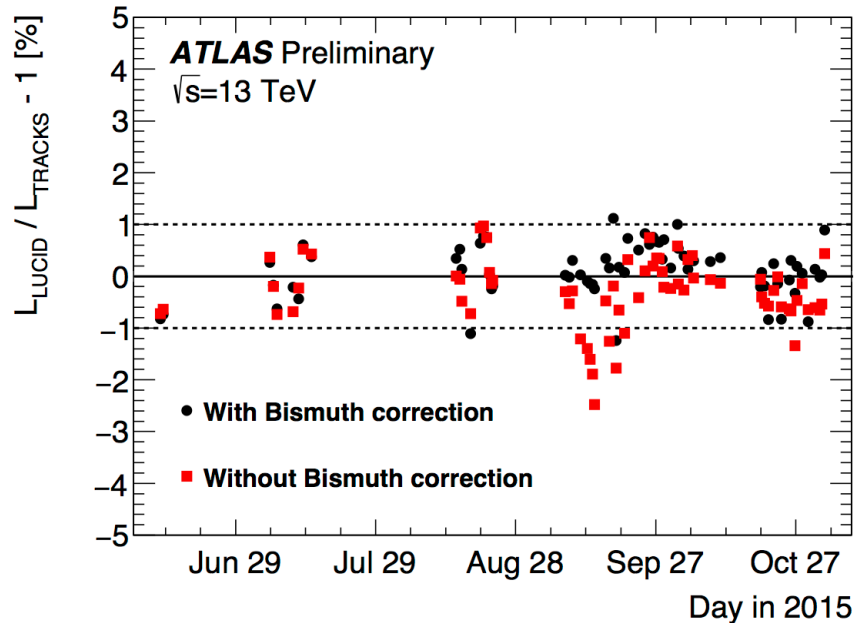
50



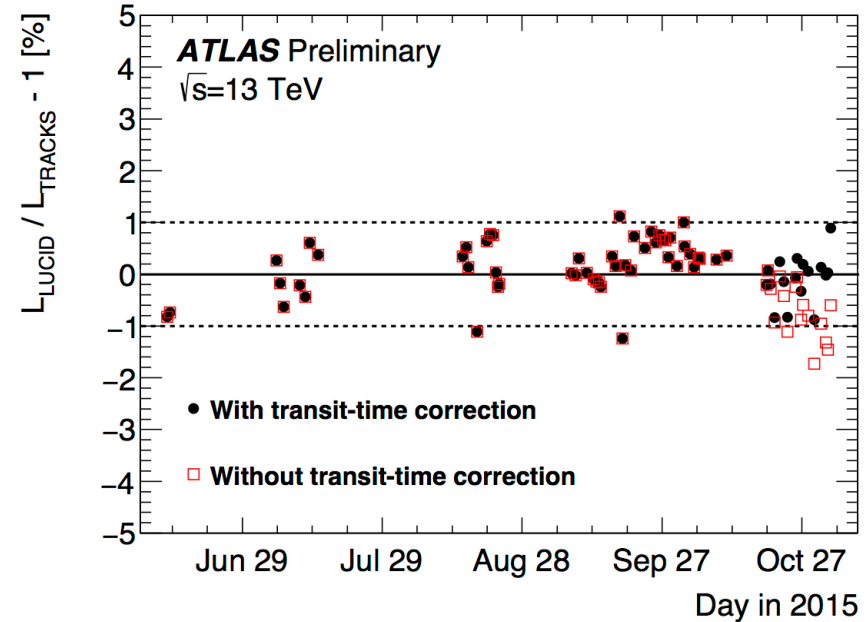
Bi207 calibration stability across 2016

The hard path towards \mathcal{L} stability: e.g. ...

51



Fractional difference in run-integrated luminosity between the LUCID_{Bi}_Evt_ORA and track-counting algorithms. Each point corresponds to an ATLAS run recorded during 50 ns or 25 ns bunch-train running in 2015 at $\sqrt{s} = 13$ TeV. Radioactive Bi-207 sources are used to monitor the gain of the PMTs in frequent calibration runs during the year. These pulse-height measurements are used to adjust the high voltage so that the gain remains constant throughout the year. In a second step, the Bi-207 calibrations are also used offline to correct the measured luminosity. The Figure shows the LUCID data before (red squares) and after the offline gain correction (black circles).



Fractional difference in run-integrated luminosity between the LUCID_{Bi}_Evt_ORA and track-counting algorithms. By the end of the data-taking period, the cumulative increase in HV that had been applied during the year to keep the PMT gain constant, resulted in a significant decrease of the transit time. This, in turn, resulted in a loss of some events outside the timing window, and thereby in a decrease in detector efficiency. The impact of the transit time increase was different for different PMTs and was negligible for one of them. This PMT was used to correct the luminosity measured by the others. The Figure shows the LUCID data before (red squares) and after the transit-time correction (black circles).

Total \mathcal{L} systematics: ALICE example (pp, 13 TeV)

52

*Source:
ALICE Collaboration,
ALICE-PUBLIC-2016-002,
June 2016*

Source	Uncertainty
Non-factorisation	0.9%
Orbit drift	0.8%
Beam-beam deflection	0.8%
Dynamic β^*	0.3%
Background subtraction	0.1% (T0), 0.7% (V0)
Pileup	0.7%
Length-scale calibration	0.5%
Fit model	0.6%
$h_x h_y$ consistency (T0 vs V0)	0.6%
Luminosity decay	0.4%
Bunch-by-bunch consistency	< 0.1%
Scan-to-scan consistency	< 0.1%
Beam centring	< 0.1%
Bunch intensity	0.6%
Total on visible cross section	2.05% (T0), 2.16% (V0)
Stability and consistency	0.6% (isolated bunches) 2.7% (whole 2015)
Total on luminosity	2.2% (isolated bunches) 3.4% (whole 2015)

Total \mathcal{L} systematics: CMS example (pp, 13 TeV)

53

Table 1: Summary of the systematic uncertainties entering the CMS luminosity measurement for 13 TeV proton-proton collisions. When applicable, the percentage correction is shown.

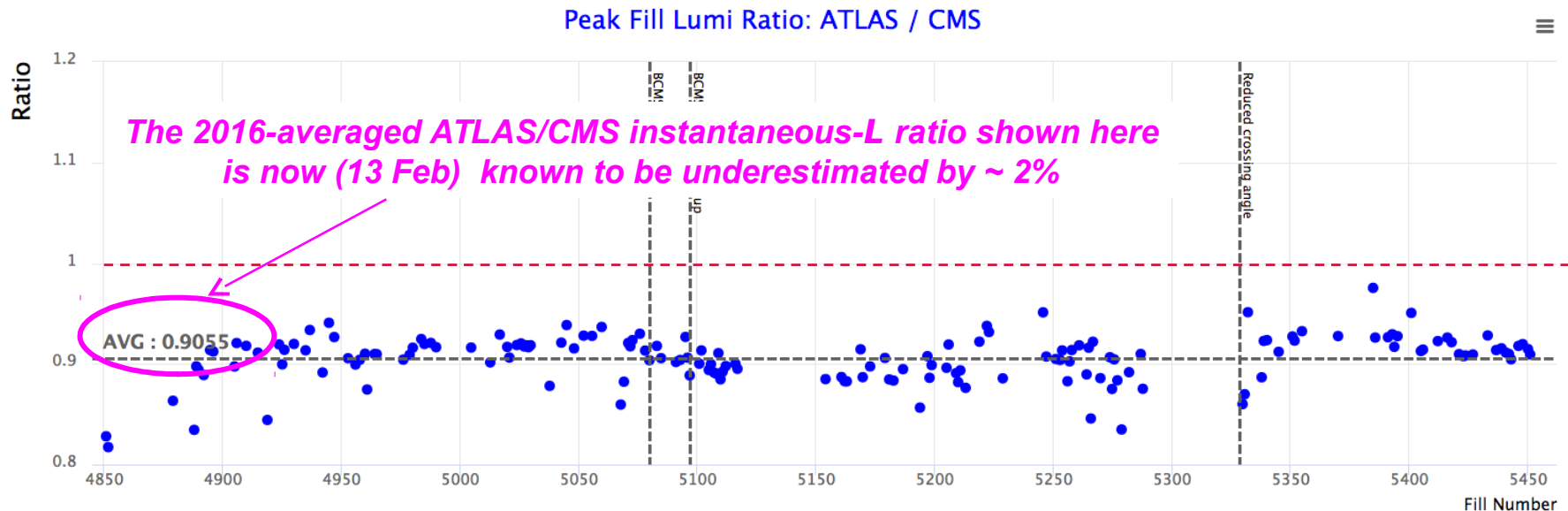
	Systematic	correction (%)	uncertainty (%)
Integration	Stability	-	1
	type 1	7 – 9	0.6
	type 2	0 – 4	0.7
	CMS deadtime	-	0.5
	Dynamic Inefficiency	-	0.4
Normalization	XY-Correlations	1.1	1.5
	Beam current calibration	-	0.3
	Ghosts and satellites	-	0.2
	Length scale	-3.2	1.5
	Orbit Drift	-	0.4
	Beam-beam deflection	1.8	0.4
	Dynamic- β	-	0.5
	Total		2.7

Source: CMS PAS LUM-15-001, March 2016

ATLAS/CMS Luminosity ratio



- Significant (~ 10%) ATLAS-CMS luminosity difference across 2016



- At least 2 identified sources
 - Largest contribution from emittance $\epsilon_x > \epsilon_y$ coupled with horizontal (x) crossing in CMS vs. vertical (y) crossing in ATLAS
 - CMS vdM analysis: recently established that L_{CMS} overestimated by ~ 3%
- Analysis complicated by residual μ -dependence of online L-data

Crossing-angle basics

- In the presence of a non-zero crossing angle θ_c in plane T (T = x, y), the luminosity is degraded by a geometric factor $F_T(\theta_c, \sigma_T/\sigma_z) < 1$
 - ⊙ σ_T = transverse single-beam size in crossing plane (y/x at IP1/IP5)
 - ⊙ σ_z = bunch length (same at IP1 & IP5)

$$\mathcal{L}_b = f_r n_1 n_2 2c \int \rho_1 \rho_2 dx dy dz dt = \frac{f_r n_1 n_2}{2\pi \Sigma_x \Sigma_y}$$

$$\Sigma_x = \sqrt{(\sigma_{\hat{x}1}^2 + \sigma_{\hat{x}2}^2) \cos^2 \alpha + (\sigma_{\hat{z}1}^2 + \sigma_{\hat{z}2}^2) \sin^2 \alpha} \quad \Sigma_y = \sqrt{\sigma_{\hat{y}1}^2 + \sigma_{\hat{y}2}^2}$$

for a half-crossing angle α (aka θ_c) in the x-plane, and where $\sigma_{x,y,z}$ are the single-beam sizes.

- **Ideal machine:** $\sigma_{x,IP1}^* = \sigma_{y,IP1}^* = \sigma_{x,IP5}^* = \sigma_{y,IP5}^*$
- There is evidence from analysis of beam-profile measurements + accelerator calculations+ history of measured ATLAS/CMS \mathcal{L} ratio that

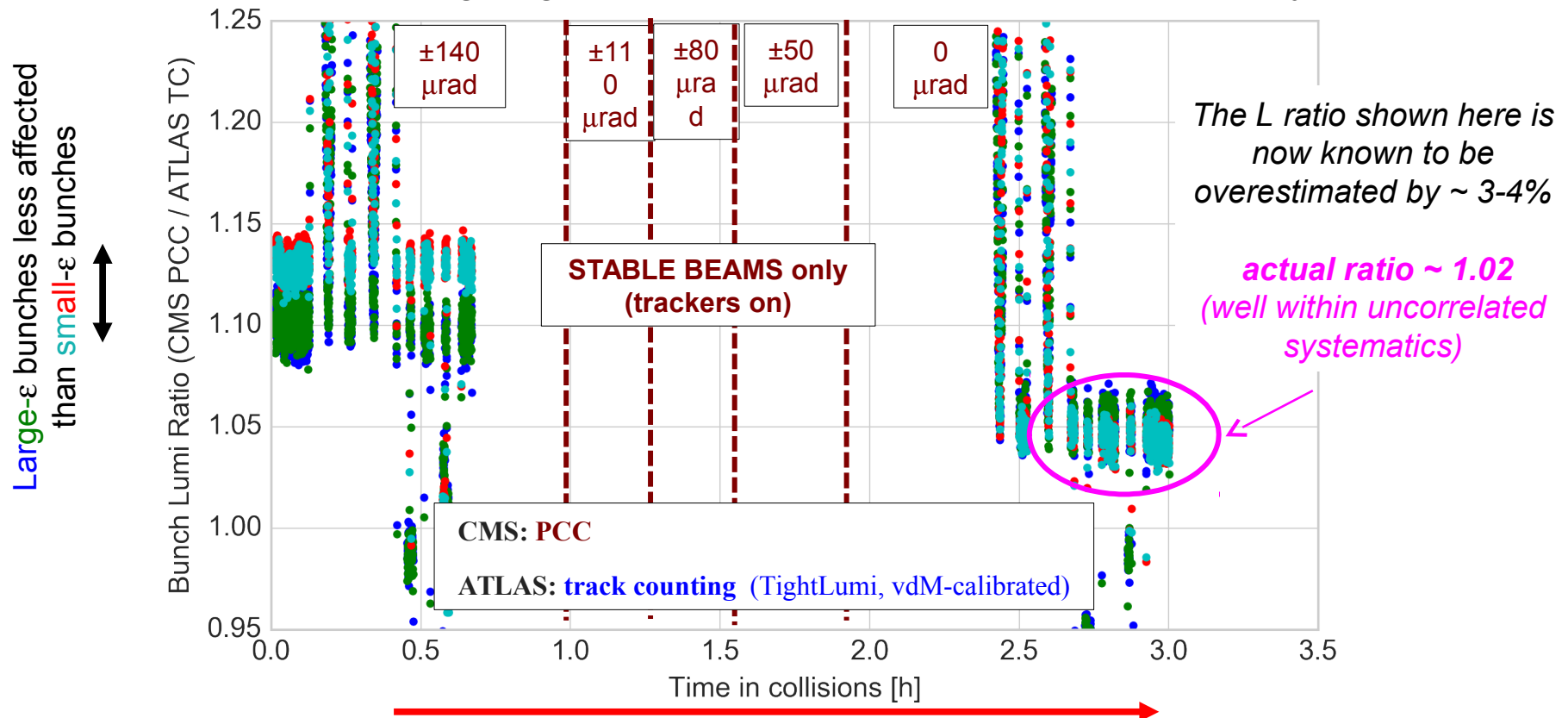
$$\varepsilon_x > \varepsilon_y \rightarrow \sigma_x^* > \sigma_y^* \rightarrow F_y [\text{IP1}] < F_x [\text{IP5}]$$

$$\mathcal{L} [\text{IP1}] / \mathcal{L} [\text{IP5}] \sim F_y [\text{IP1}] / F_x [\text{IP5}]$$

Crossing-angle scan: L_{ATL} / L_{CMS}



- Effect confirmed by dedicated crossing angle scan
 - measure crossing angle dependence of ATLAS/CMS luminosity ratio



- Clear **effect from changing crossing angle** on ATLAS/CMS luminosity ratio
- However quantitative agreement with prediction not yet satisfactory

57

Attic